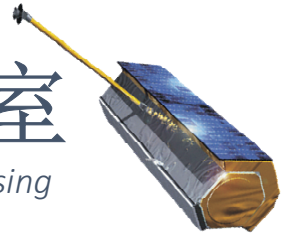




测绘遥感信息工程国家重点实验室

State Key Laboratory of Information Engineering in Surveying, Mapping and Remote Sensing



Synthetic Aperture Radar Tomography – practical course

Timo Balz, Stefano Tebaldini, Laurent Ferro-Famil



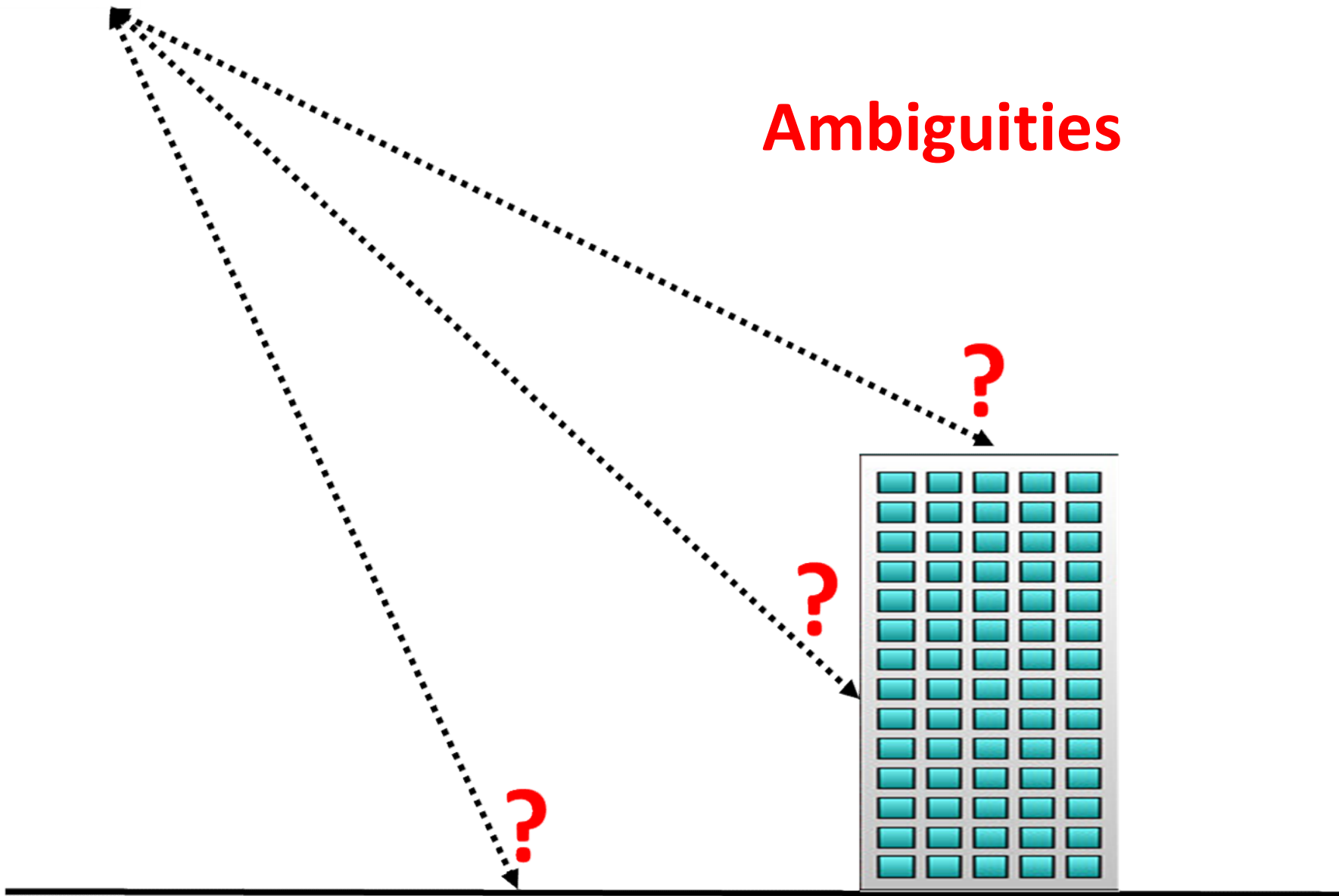
TomoSAR_Main.m

```
%%%%%%%%%%%%%%%%%%%%%%%%%%%%%%%%%%%%%%%%%%%%%%%%%%%%%%%%%%%%%%%%%%%%%%%%%%%%%%  
%%%%%%%%%%%%%%%%%%%%%%%%%%%%%%%%%%%%%%%%%%%%%%%%%%%%%%%%%%%%%%%%%%%%%%%%%%%%%%  
% DEMONSTRATIVE TOMOGRAPHIC SAR PROCESSING FOR FOREST ANALYSIS  
% AUTHOR: STEFANO TEBALDINI, POLITECNICO DI MILANO  
% EMAIL: stefano.tebaldini@polimi.it  
% TEL: +390223993614  
%  
% THE FOLLOWING SCRIPT AND ALL RELATED SCRIPTS/FUNCTIONS AND DATA ARE INTENDED AS  
% MATERIAL FOR THE TOMOSAR TRAINING COURSE HELD IN BEIJING IN FEBRUARY 2015  
% BY LAURENT FERRO-FAMIL AND STEFANO TEBALDINI  
%  
% THIS SOFTWARE WAS DEVELOPED AND TESTED USING MATLAB R2011b  
%  
% SAR DATA USED IN THIS SCRIPT ARE PART OF THE SAR DATA-SET ACQUIRED BY DLR  
% IN 2008 IN THE FRAME OF THE ESA CAMPAIGN BIOSAR 2008  
% DATA FOCUSING, COREGISTRATION, PHASE FLATTENING, AND GENERATION OF KZ  
% MAPS WERE CARRIED OUT BY DLR.  
% DATA PHASE CALIBRATION WAS CARRIED OUT BY THE AUTHOR  
%  
% TERRAIN ELEVATION DATA USED IN THIS SCRIPT ARE EXTRACTED FROM  
% THE LIDAR DATA-SET ACQUIRED BY THE SWEDISH DEFENCE RESEARCH AGENCY (FOI)  
% AND HILDUR AND SVEN WINQUIST'S FOUNDATION IN THE FRAME OF THE ESA  
% CAMPAIGN BIOSAR 2008  
% PROCESSING OF LIDAR DATA AND PROJECTION ONTO SAR GEOMETRY WAS CARRIED OUT  
% BY THE AUTHOR  
%  
% YOU ARE WELCOME TO ADDRESS ME QUESTIONS/COMMENTS/CORRECTIONS AT  
% stefano.tebaldini@polimi.it  
%%%%%%%%%%%%%%%%%%%%%%%%%%%%%%%%%%%%%%%%%%%%%%%%%%%%%%%%%%%%%%%%%%%%%%%%%%%%%%  
%%%%%%%%%%%%%%%%%%%%%%%%%%%%%%%%%%%%%%%%%%%%%%%%%%%%%%%%%%%%%%%%%%%%%%%%%%%%%%
```



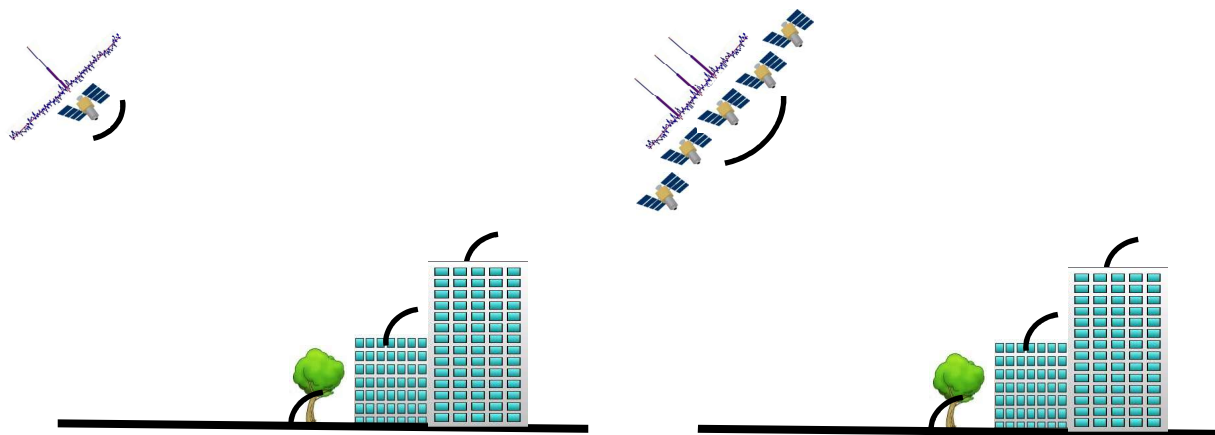


Ambiguities

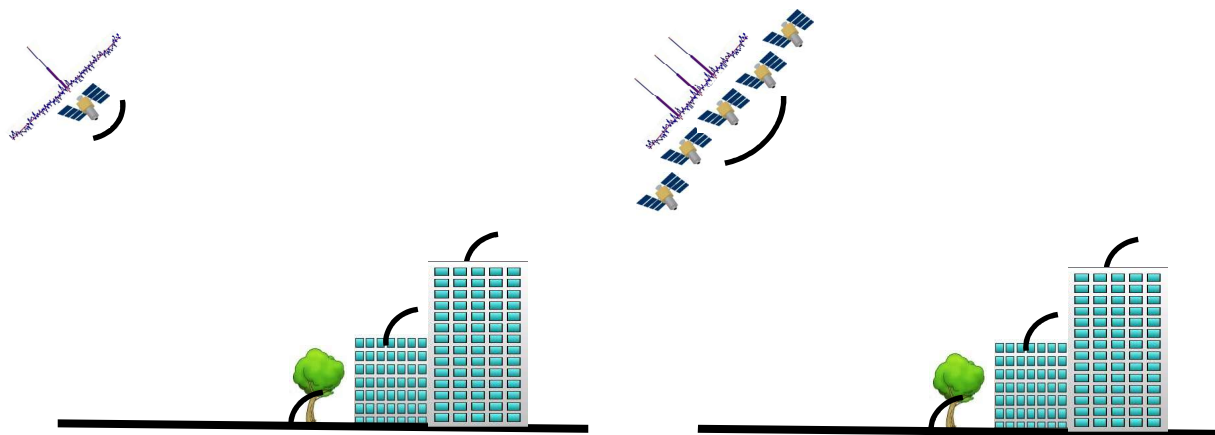




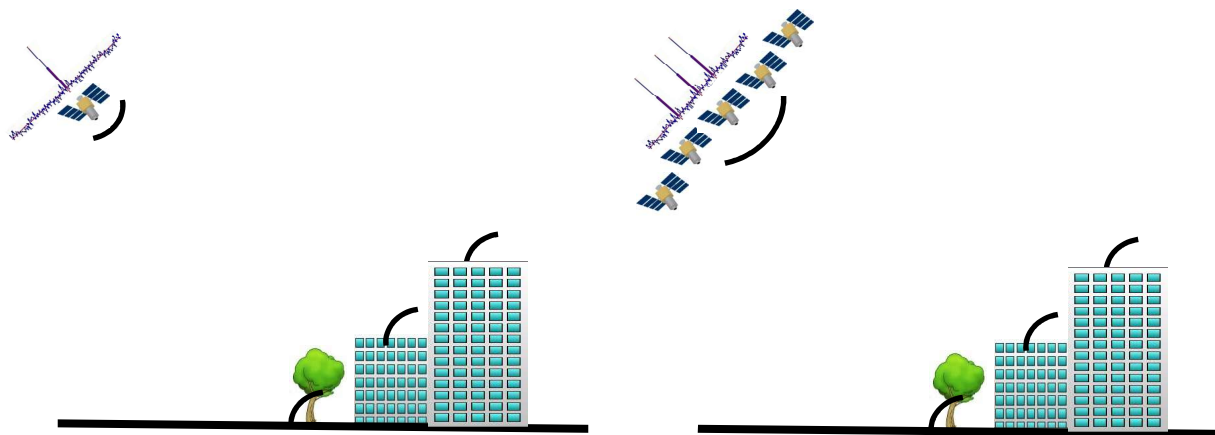
TomoSAR principle



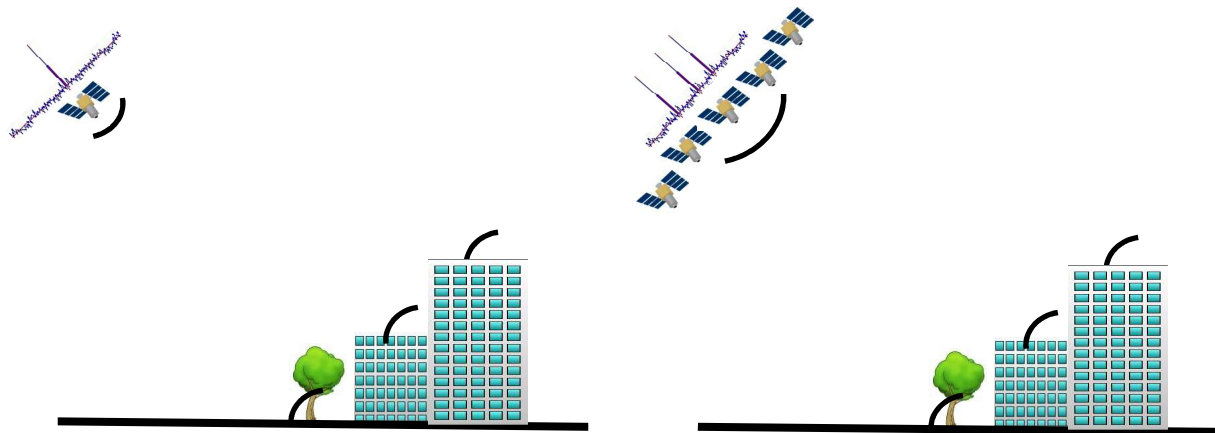
TomoSAR principle



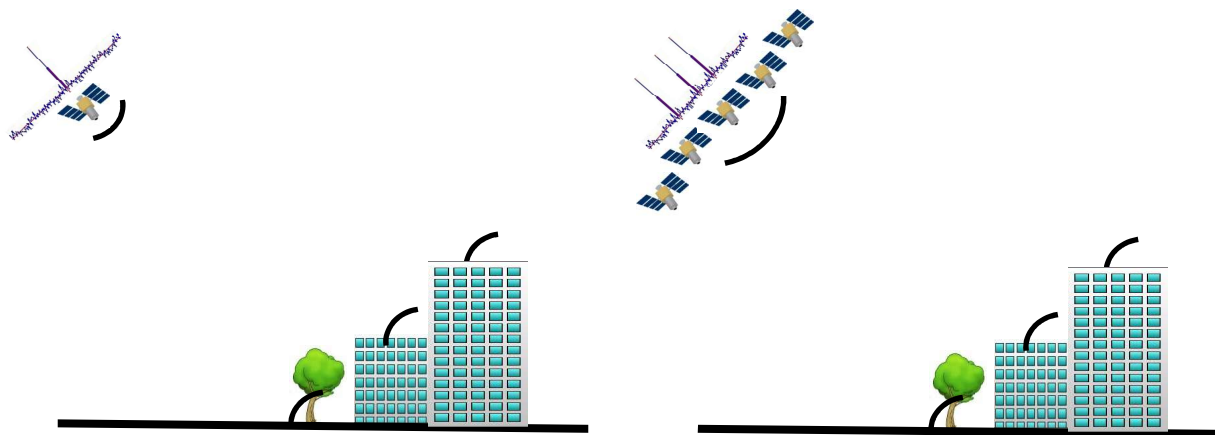
TomoSAR principle



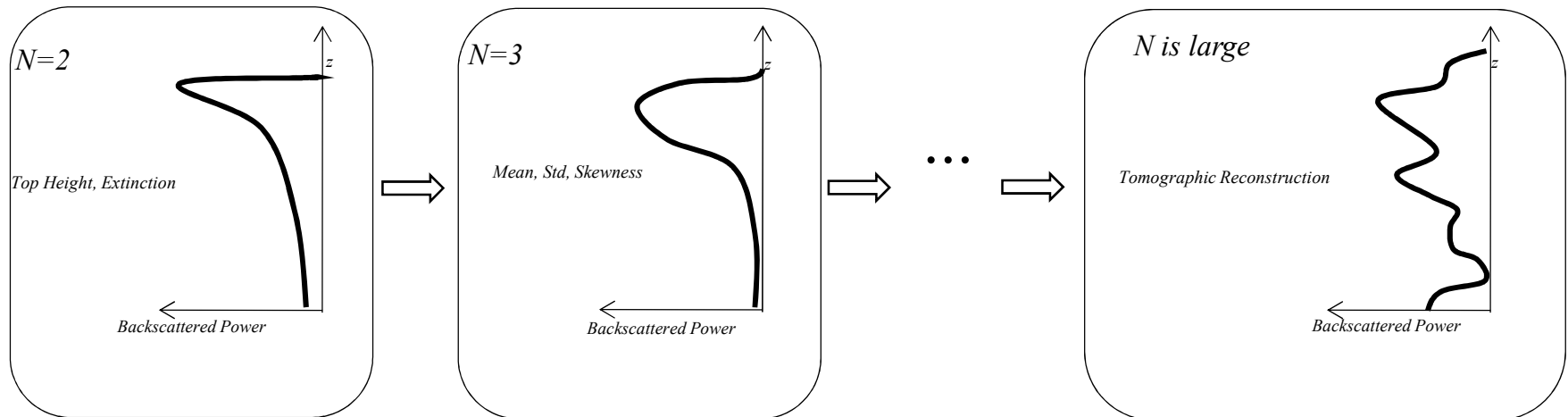
TomoSAR principle



TomoSAR principle



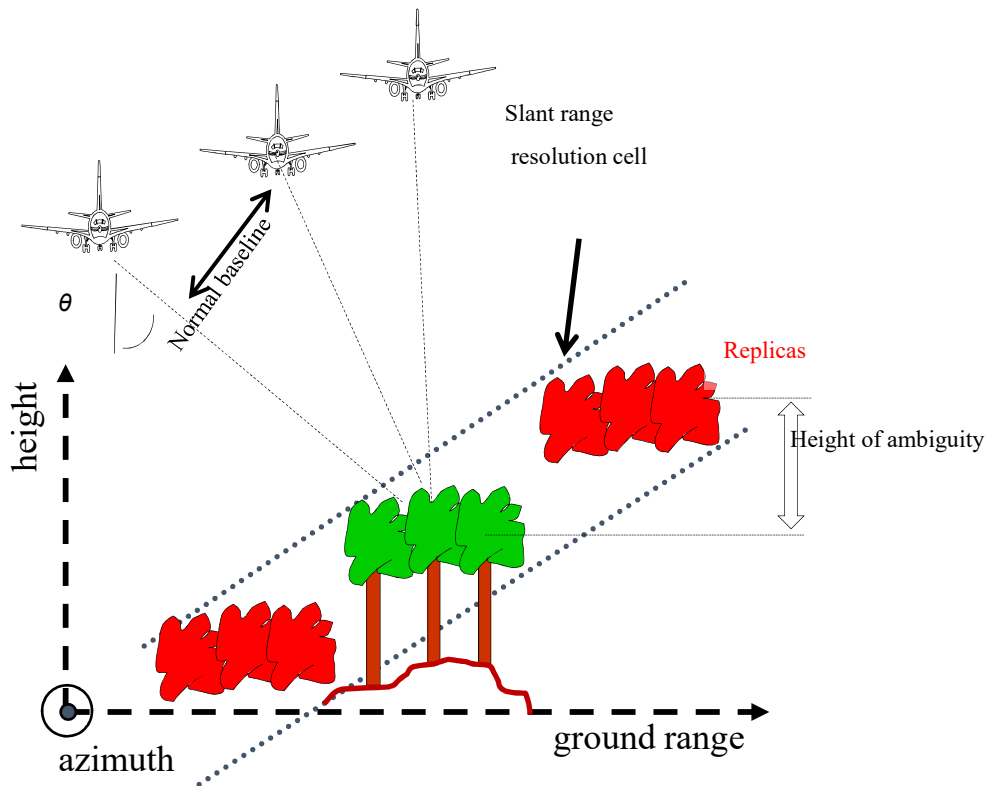
- Why multiple baselines?
 - Because: **more equations!**
 - Increased robustness against disturbances (temporal decorrelation...)
 - and/or relaxation of hypotheses required in the single baseline case
 - more unknowns are available to characterize the vertical structure of the scene



MB allow to pass from model-based inversion to full tomographic reconstruction

Rationale: Form a 2D synthetic aperture by collecting multiple SAR acquisitions acquired along parallel flight lines

- Vertical resolution \Leftrightarrow total normal baseline span
- Vertical ambiguity \Leftrightarrow normal baseline spacing



Multi-baseline (MB) systems:

- Multiple pass systems:
airborne and spaceborne SARs
 - Multiple antenna systems:
ground based Radars
- MB campaigns involve:
- Higher costs:
spaceborne: $\approx x 1$
ground based: $\approx x N$
 - More sophisticated processing:
see single vs multi-baseline InSAR...

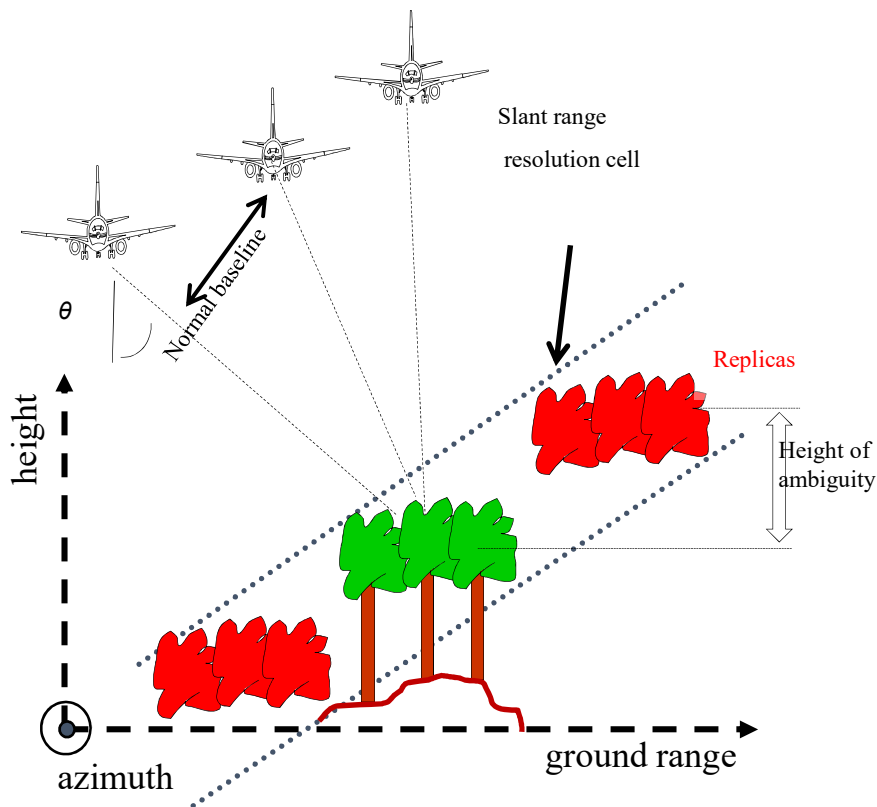
Source:
Tebaldini & Rocca



Tomographic SAR

Rationale: Form a 2D synthetic aperture by collecting multiple SAR acquisitions acquired along parallel flight lines

- Vertical resolution \Leftrightarrow total normal baseline span
- Vertical ambiguity \Leftrightarrow normal baseline spacing



Multi-baseline (MB) systems:

- Multiple pass systems:
airborne and spaceborne SARs
- Multiple antenna systems:
ground based Radars

MB campaigns involve:

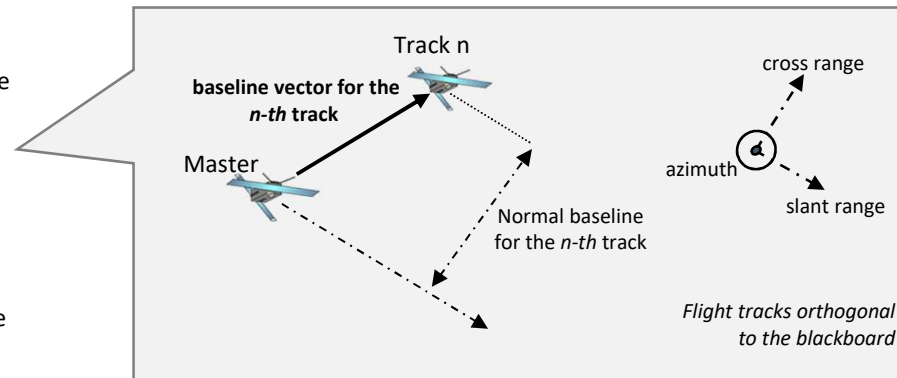
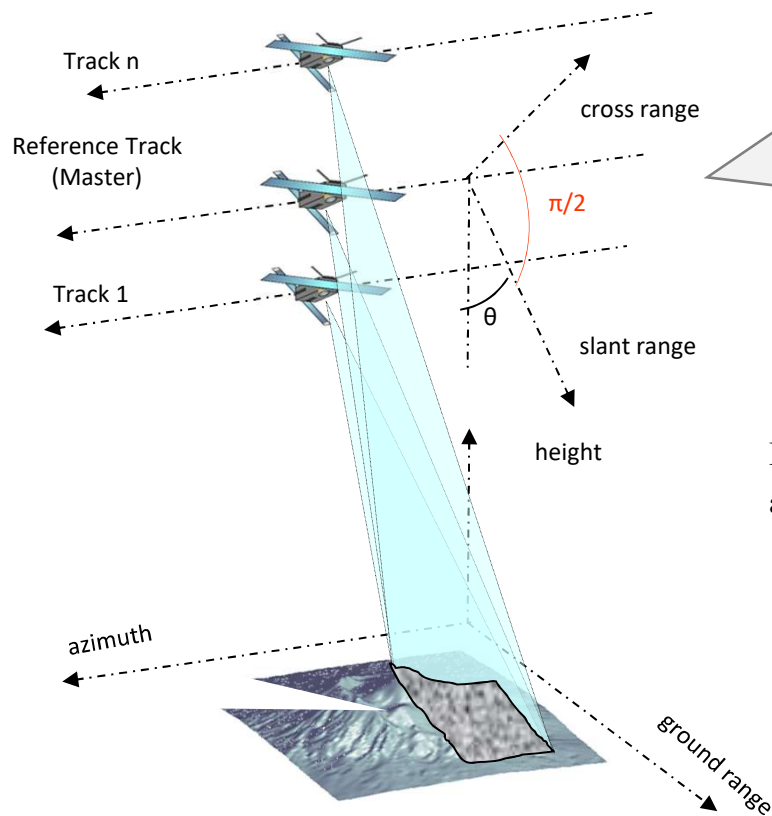
- Higher costs:
spaceborne: $\approx x 1$
ground based: $\approx x N$
- More sophisticated processing:
see single vs multi-baseline InSAR...

Source: Tebaldini & Rocca



Basic concepts

Multiple baselines \Leftrightarrow Illumination from multiple points of view



By collecting several baselines it is possible to synthesize an antenna along the cross range direction as well

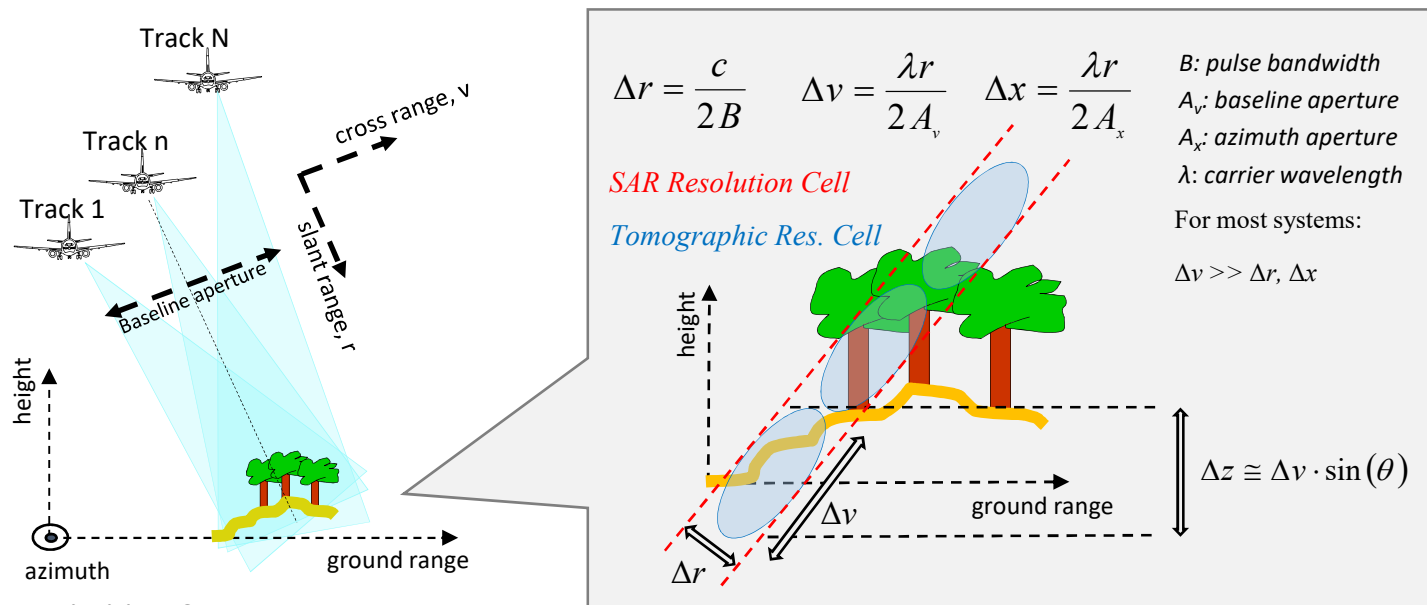


3D focusing is possible in the coordinate system: *slant range, azimuth, cross range*

Basic concepts

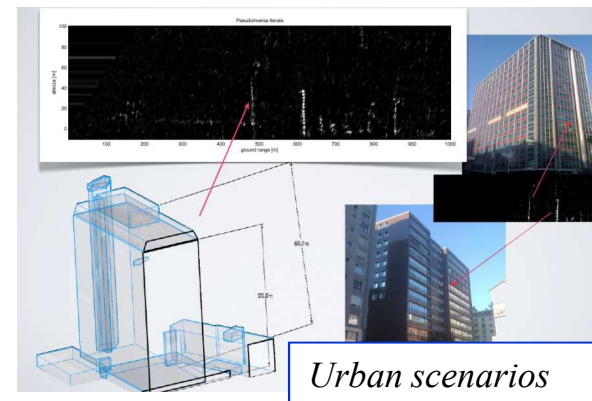
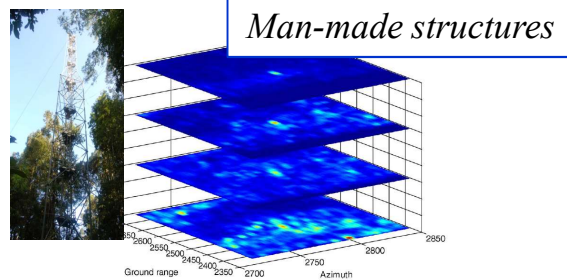
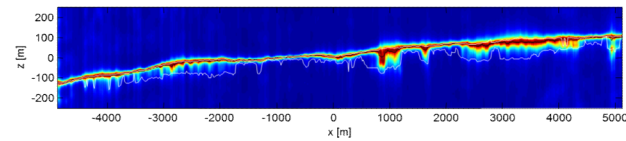
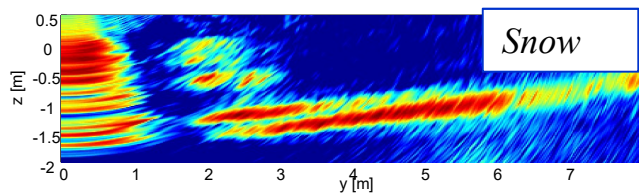
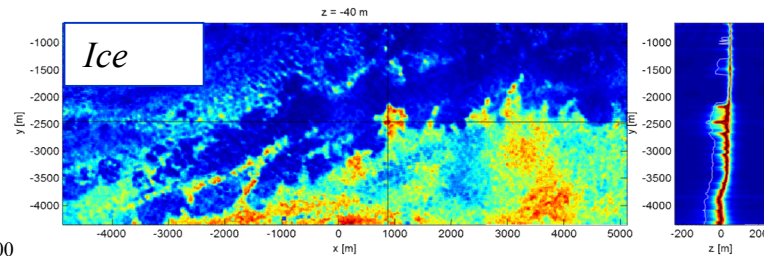
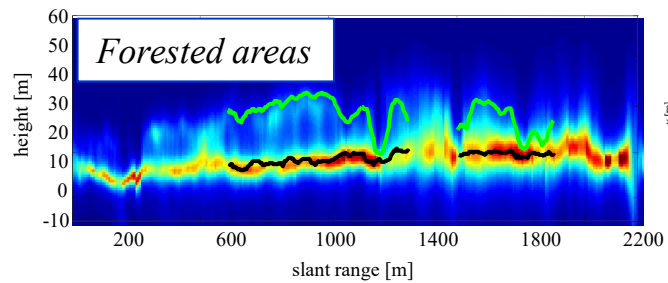
Resolution is determined by pulse bandwidth along the slant range direction, and by the lengths of the synthetic apertures in the azimuth and cross range directions

⇒ The SAR resolution cell is split into **multiple layers**, according to baseline aperture

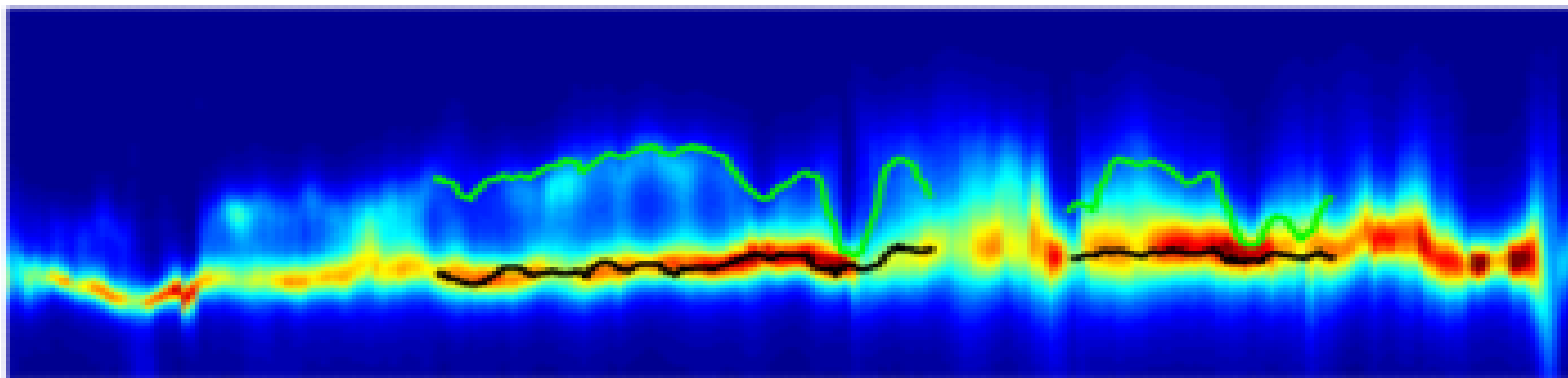
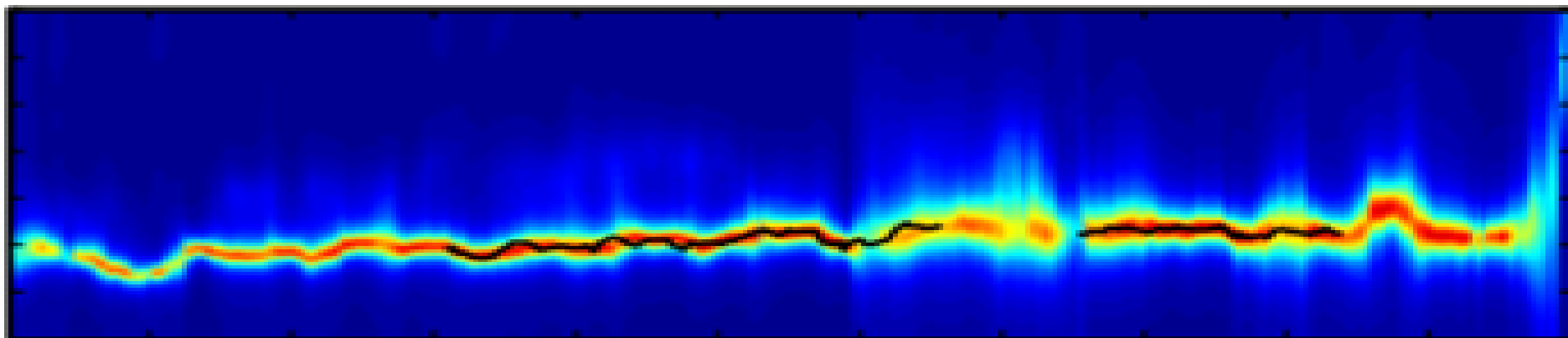


Source: Tebaldini & Rocca

TomoSAR gives access to the 3D structure



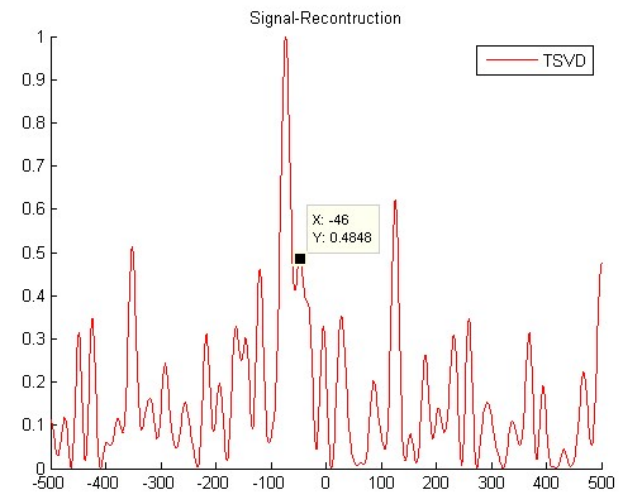
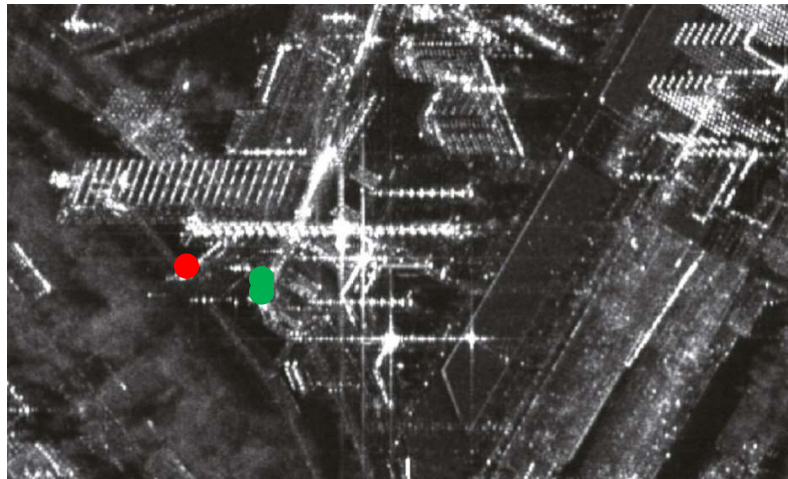
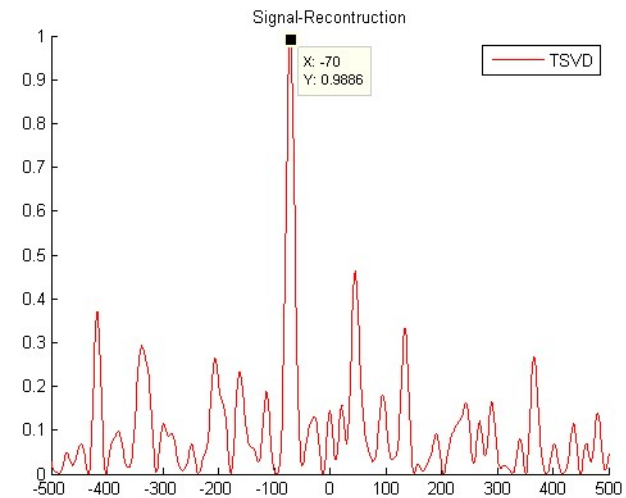
Polarimetric TomoSAR over Vegetation



Foliage penetration

Biomass estimation

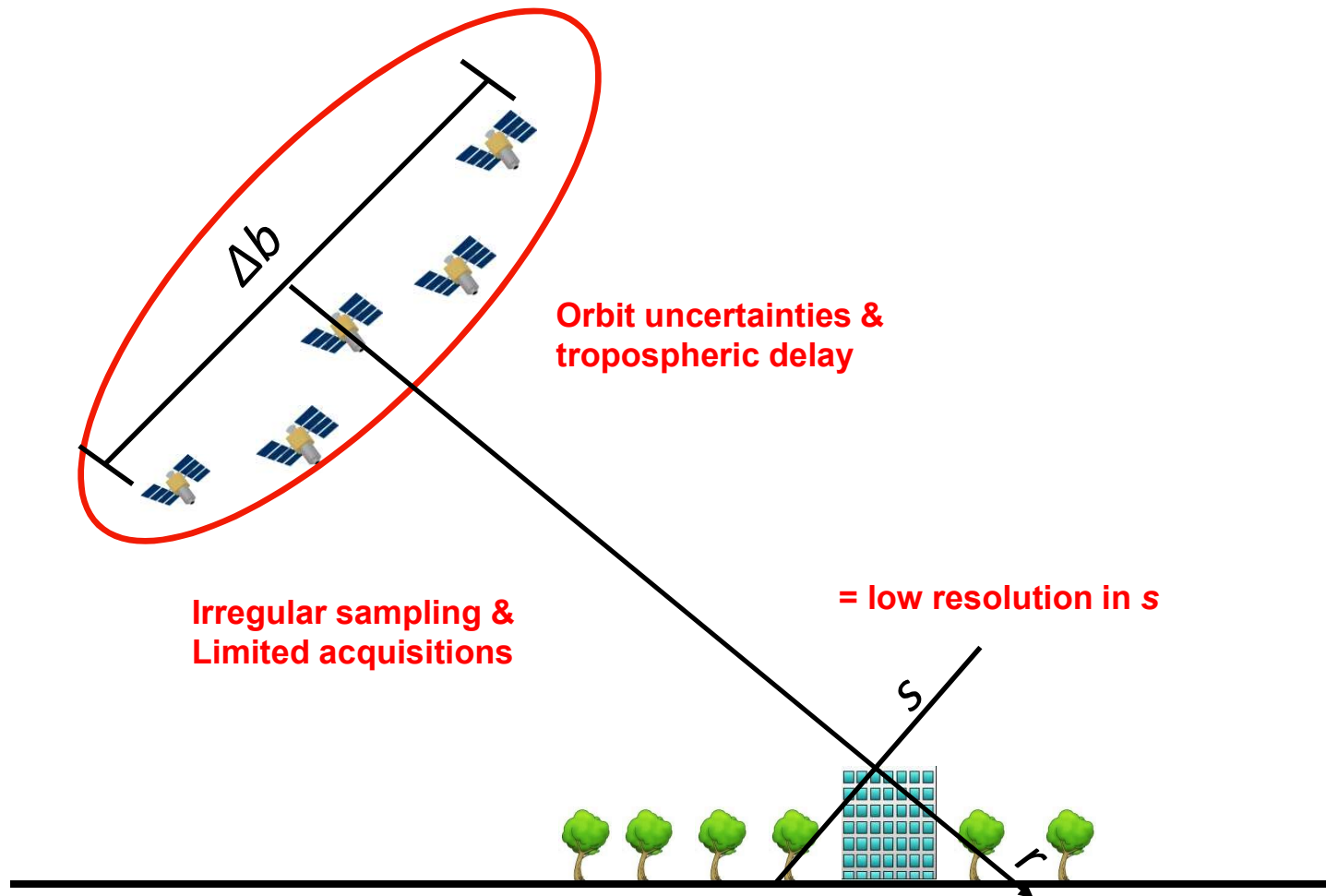
Urban TomoSAR



Finite number of scatterers



TomoSAR principle



TomoSAR as spectral estimation problem

$$g_n = \int_{-a}^a \gamma'(s) \exp \left[-j2\pi \left(-\frac{2}{\lambda} \frac{b_{\perp n}}{|r_0 - b_{\parallel n}|} \right) s \right] ds$$

where

$$\gamma'(s) = \gamma(s) \exp \left[-j \frac{4\pi}{\lambda} \frac{s^2}{2|r_0 - b_{\parallel n}|} \right]$$

so, g_n is the Fourier transformation of $\gamma'(s)$ at position

$$f_n = -\frac{2b_{\perp n}}{\lambda|r_0 - b_{\parallel n}|} \approx -\frac{2b_{\perp n}}{\lambda r}$$

TomoSAR basics

The focused SAR image from the n^{th} pass of a specific cell is nothing else but the Fourier Transfer of the reflectivity function in the elevation direction at the position

$$g_n = \int_{-a}^a \gamma(s) \exp[-j2\pi f_n s] ds = FT[\gamma(s)]|_{f_n} = g(f)|_{f_n}$$



TomoSAR basics

The expected resolution in elevation p_s depends on the slant-range r and the aperture size in elevation Δb

$$p_s = \frac{\lambda r}{2\Delta b}$$

The extent of the illuminated objects and therefore the limits of the extent in elevation Δs depends on r , Δb , and the resolution in range p_r . In the spaceborne case, with large slant-range r , this is seldom a limitation (see Zhu & Bamler, 2010).

$$\Delta s \ll \frac{p_r r}{\Delta b}$$

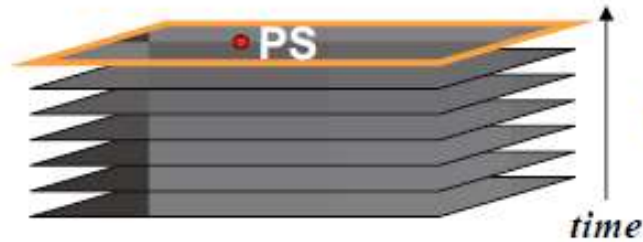


PS-InSAR for pre-processing

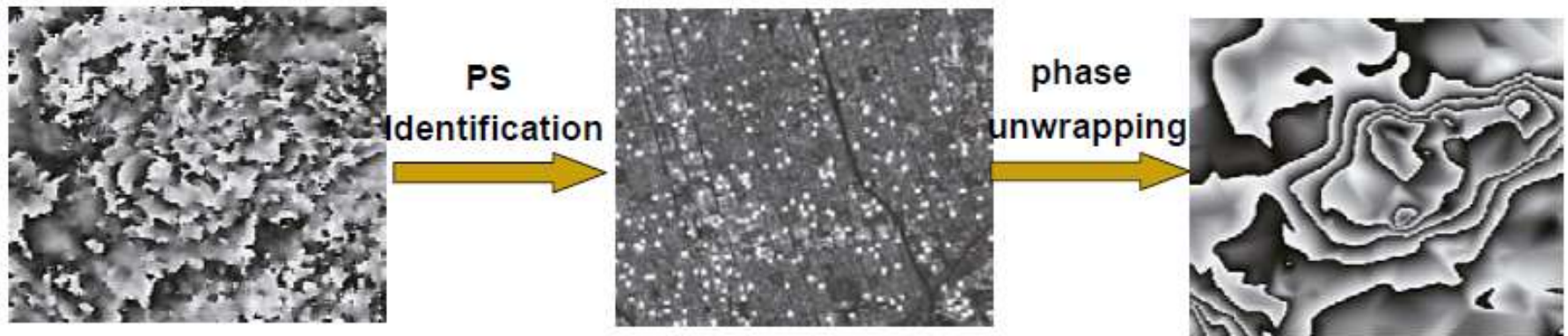
- Using TomoSAR on a large area requires the removal of atmospheric effects
- This can be done using PS-InSAR
 - However, this requires a large number of PS to be found
 - Therefore, this works best in urban areas
- PS-InSAR is used for pre-processing
- Afterwards, TomoSAR can be used



PS-InSAR



Those scatterers (called PS) that are coherently observed by the radar during a long period of are identified from a few tens of SAR images.



- Finding stable point-like targets --- Permanent Scatterers
- Interpolating atmosphere affection and remove it
- Estimate the elevation and deformation on PS



PS-InSAR steps

- Import
- Selection of the master image
- Co-Registration
 - Typically to a single-master
- Interferogram processing
 - Not in every implementation. Several PS-InSAR implementations only use the phases of the PS candidates
- PS candidates selection
- APS estimation
 - Typically on a subset of the PS candidates
- *PS point processing*
- *Post-processing*
- *Visualization*



Image co-registration

- Identical to the co-registration described in the InSAR section:
- Registration accuracy < 0.2 pixel is required
 - This requirement is even much higher during TOPS processing
- Different methods available
 - Based on the amplitude
 - Based on complex data – searching maximal coherence
- Slave images are resampled to the master image
- Results need to be checked and the parameters may need to be adjusted



PS candidate selection

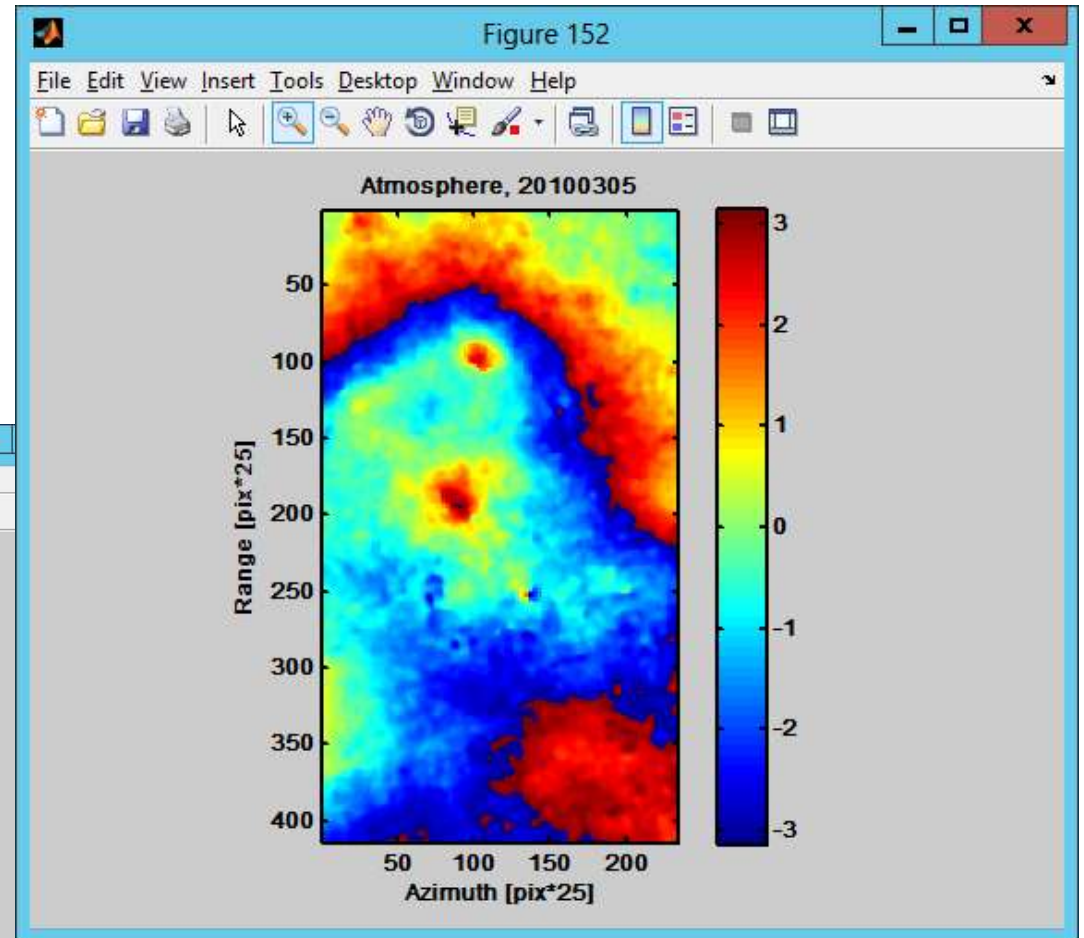
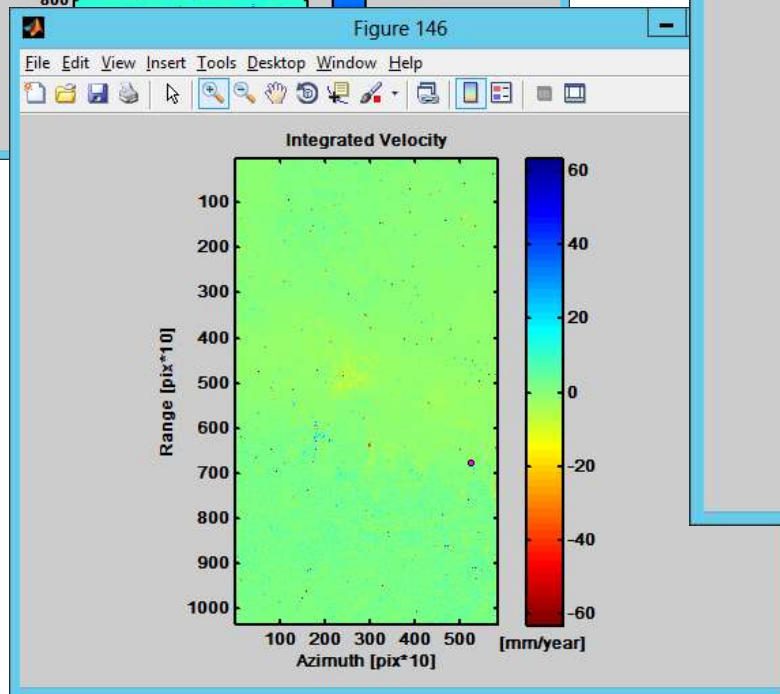
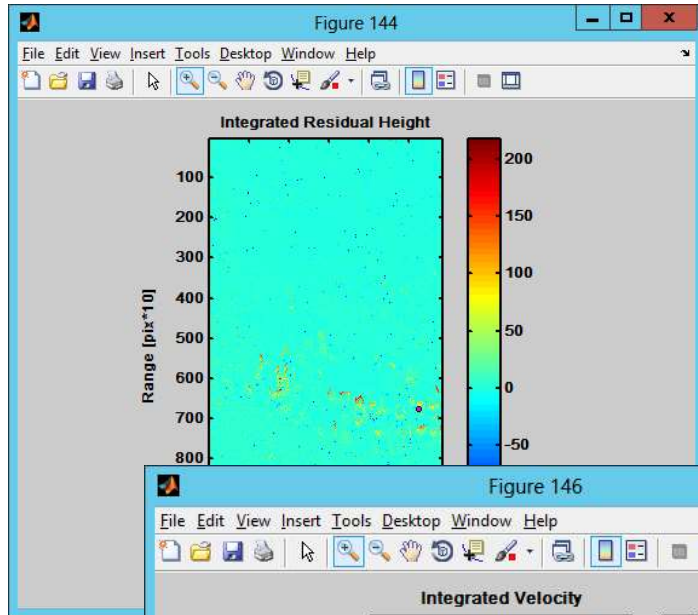
- Classical way: amplitude dispersion index

$$d_a = \frac{StdDev_a}{Mean_a}$$

- Other possible ways, e.g. based on coherence
- Be aware: amplitude dispersion index not ideal for TomoSAR, because the existence of several scatterers in a resolution cell can increase the index



APS estimation



Example: SARProZ



Spectral estimators

- **Beamforming:**

inverse Fourier Transform; coarse spatial resolution; radiometrically consistent

$$\hat{S}(v) = \mathbf{a}^H(v) \hat{\mathbf{R}} \mathbf{a}(v) \quad \mathbf{a}(v) = \left[\exp\left(j \frac{4\pi}{\lambda r} b_1 v\right) \quad \exp\left(j \frac{4\pi}{\lambda r} b_2 v\right) \quad \dots \quad \exp\left(j \frac{4\pi}{\lambda r} b_N v\right) \right]^T$$

- **Capon Spectral Estimator:**

spatial resolution is greatly enhanced, at the expense of radiometric accuracy;

$$\hat{S}(v) = \frac{1}{\mathbf{a}^H(v) \hat{\mathbf{R}}^{-1} \mathbf{a}(v)}$$

- **Methods based on the analysis of the Eigenstructure of \mathbf{R} (MUSIC, ESPRIT...):**

determination of the dominant scattering centers; mostly suited for urban scenarios

- **Methods based on sectorial information (Truncated SVD, PCT...):**

optimal basis choice (e.g.: Legendre), depending on a-priori info about the scene vertical extent

- **Model based methods (NLS, COMET...):**

model based; high radiometric accuracy; high computational burden; possible model mismatches

- **Compressive sensing:**

localization of few scattering centers via L1 norm minimization; mostly suited for urban scenarios



Multiple scatterers

$$g_n = \sum_{k=1}^{n_p} \gamma_k e^{-j2\pi f_n s_k} + v_n \quad n = 0, \dots, n_s$$

where

g_n = complex value observed for the n^{th} pass

γ_k = complex amplitude of k^{th} scatterer

s_k = elevation of k^{th} scatterer

$n_s + 1$ = number of available images

n_p = number of scatterers inside a resolution cell

v_n = noise

f_n = frequency of sampled FT which depends on the baseline



Non-linear least-square estimation

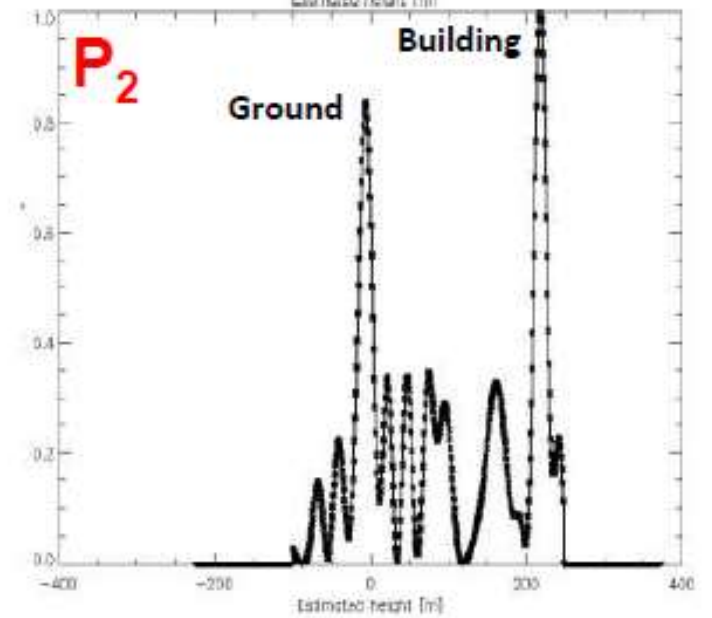
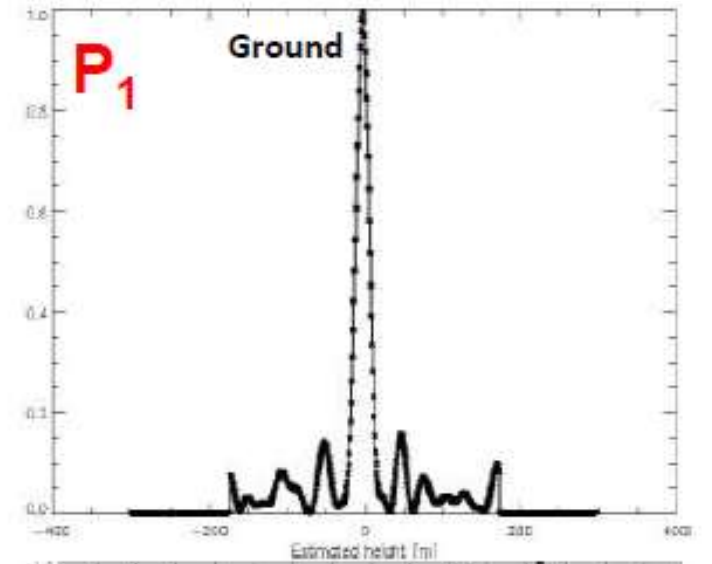
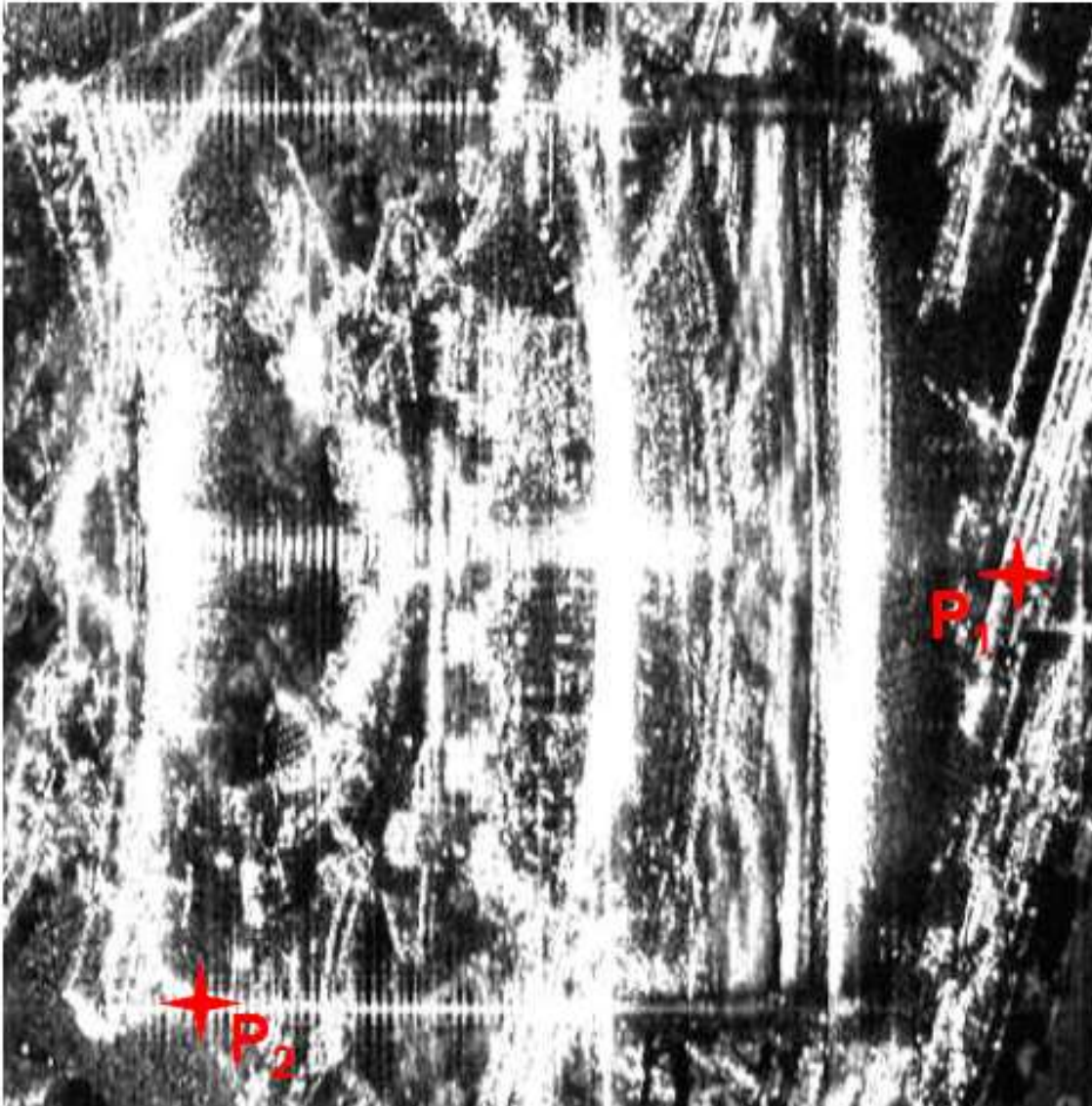
$$\vec{g} = H(\vec{s}) \cdot \vec{x} + \vec{v}$$

$$H(\vec{s}) = \begin{bmatrix} e^{2\pi f_0 s_1} & \dots & e^{2\pi f_0 s_{n_p}} \\ \vdots & & \vdots \\ e^{2\pi f_{n_s} s_1} & \dots & e^{2\pi f_{n_s} s_{n_p}} \end{bmatrix}_{(n_s+1) \times n_p}$$

$$\vec{g} = \begin{bmatrix} g_0 \\ \vdots \\ g_n \end{bmatrix}_{(n_s+1) \times 1} \quad \vec{x} = \begin{bmatrix} \gamma_1 \\ \vdots \\ \gamma_{n_p} \end{bmatrix}_{n_p \times 1} \quad \vec{v} = \begin{bmatrix} v_0 \\ \vdots \\ v_n \end{bmatrix}_{(n_s+1) \times 1}$$



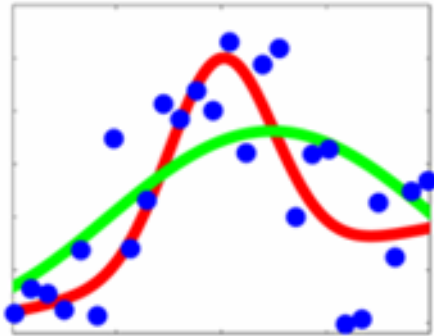
SVD on real data



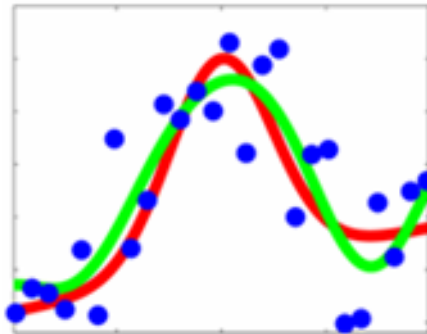
Model selection

- Selecting a statistical model for given data

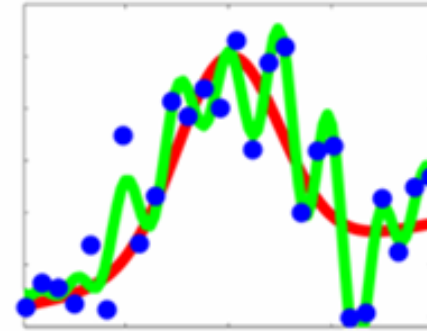
too simple –
order too low



appropriate model



too complex –
order too high



- Selecting the correct model is the model selection problem



Model selection methods

- Bayesian Information Criterion (BIC)

$$\hat{k} = \arg \max_k \left\{ \ln p(y|\hat{\theta}(k), k) - \frac{k}{2} \ln n \right\}$$

- Akaike Information Criterion (AIC)

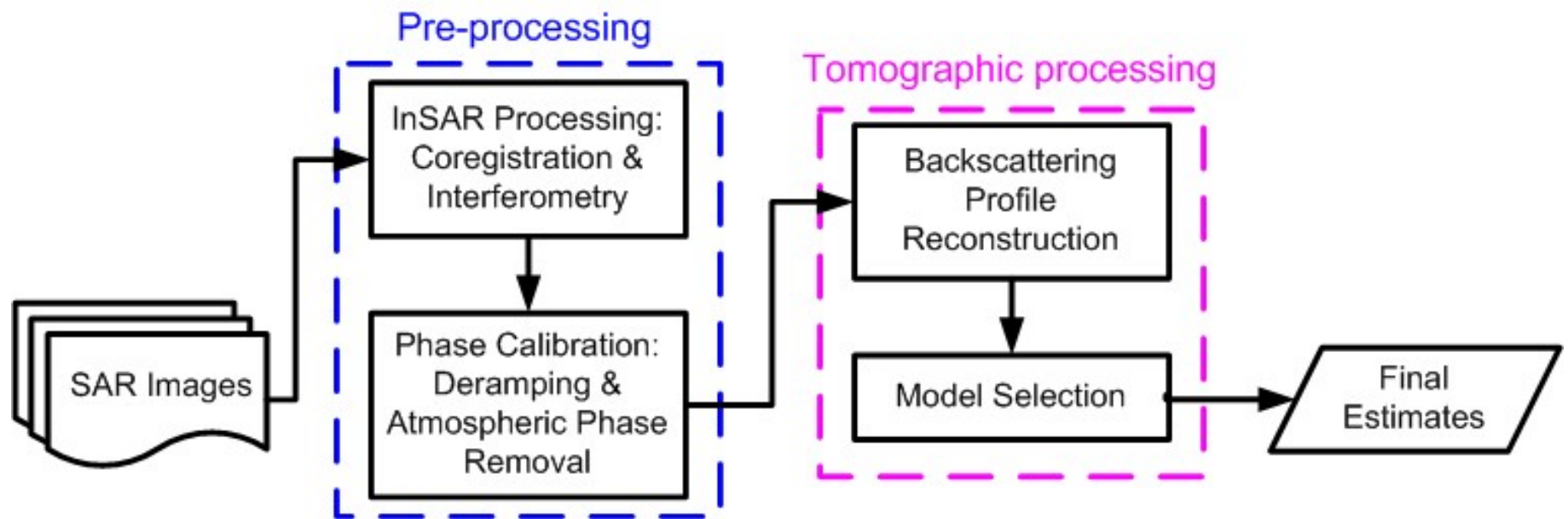
$$\hat{k} = \arg \min_k \left\{ -2 \ln p(y|\hat{\theta}(k), k) + 2k \right\}$$

- Minimum Description Length (MDL)

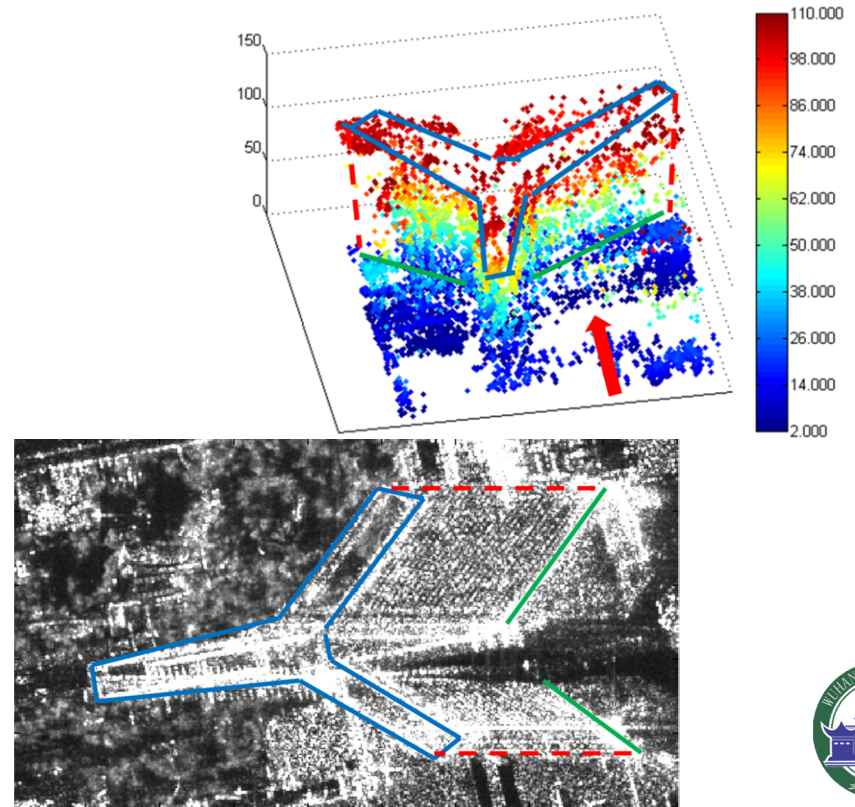
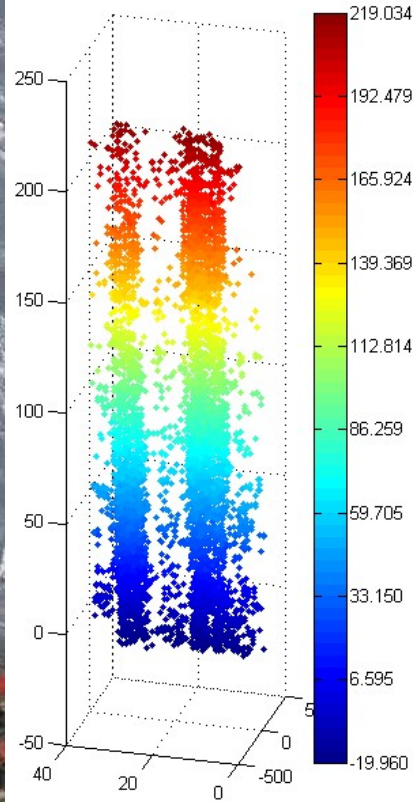
$$\hat{k} = \arg \min_k \left\{ -\ln p(y|\hat{\theta}(k), k) + \frac{k}{2} \ln n \right\}$$



TomoSAR processing steps



3D scatterer reconstruction



Urban TomoSAR different methods

- SVD based methods
 - SVD
 - Truncated SVD (T-SVD)
 - Wiener SVD
 - Butterworth-SVD
- Compressive Sensing based methods
 - Basis Pursuit (BP)
 - TWIST



TWIST

Another solution to SAR tomography is by L1 norm minimization, which is also the core of compressive sensing:

$$g = K \cdot \gamma + \varepsilon$$
$$\min \|\gamma\|_1 \text{ subject to } g = K\gamma$$

The argument listed above can be stated by

$$\Psi(\gamma) = \arg \min_{\gamma} \left\{ \frac{1}{2} \|g - K\gamma\|_2^2 + \lambda_K \|\gamma\|_1 \right\}$$

λ_K

where λ_K is a weighted value adjusted according to the noise level.



TWIST

- SAR tomography with compressive sensing
 - (see Zhu, Xiaoxiang's work in the references)
- Often, TomoSAR with compressive sensing is based on Basis Pursuit (BP)
 - Very high super-resolution
 - However, time-consuming
- Alternatively: Two-Step Iterative Shrinkage Thresholding (TWIST) for TomoSAR
 - Very efficient
 - Less super-resolution capability



TWIST

When using TWIST, the least squares fitting is needed to calculate γ_0

Calculate γ_1 according to

$$\gamma_1 = \Psi(\gamma_0 + K^T(g - K\gamma_0))$$

where Ψ is the normalization equation.

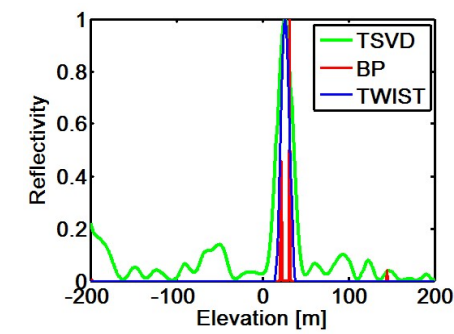
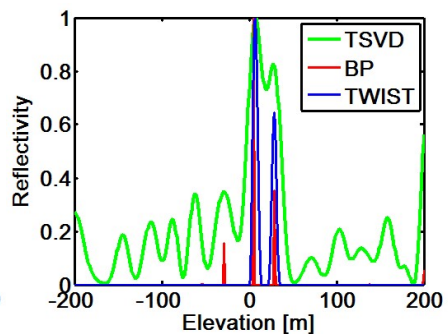
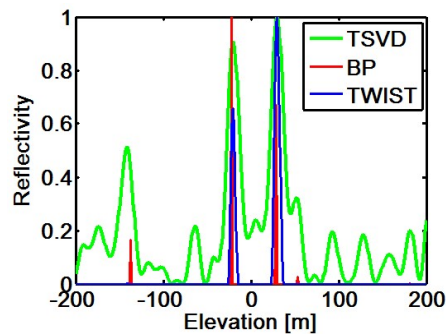
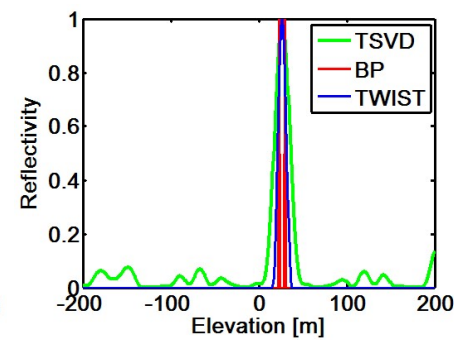
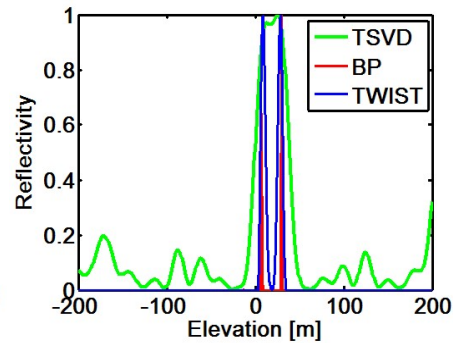
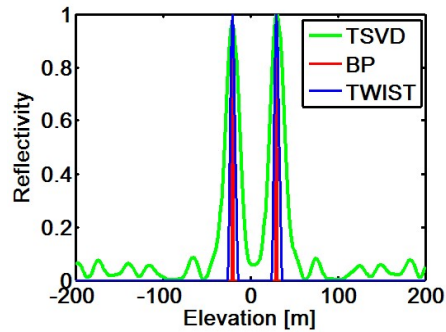
If $t \geq 1$

$$\gamma_{t+1} = (1 - \alpha)\gamma_{t-1} + (\alpha - \beta)\gamma_t + \beta \cdot \Psi(\gamma_t + K^T(g - K\gamma_t))$$

in which, α, β are the weighting coefficients



TomoSAR: different methods



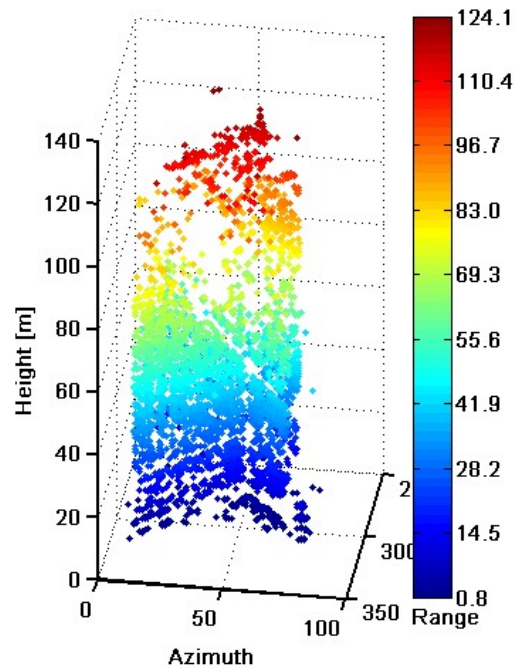
(a) $s_{Sc1}=-20m$,
 $s_{Sc2}=30m$;

(b) $s_{Sc1}=8m$,
 $s_{Sc2}=30m$;

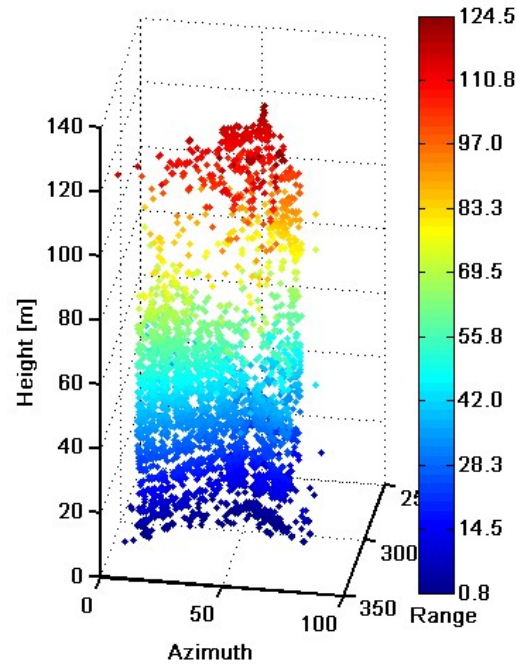
(c) $s_{Sc1}=23m$;
 $s_{Sc2}=30m$



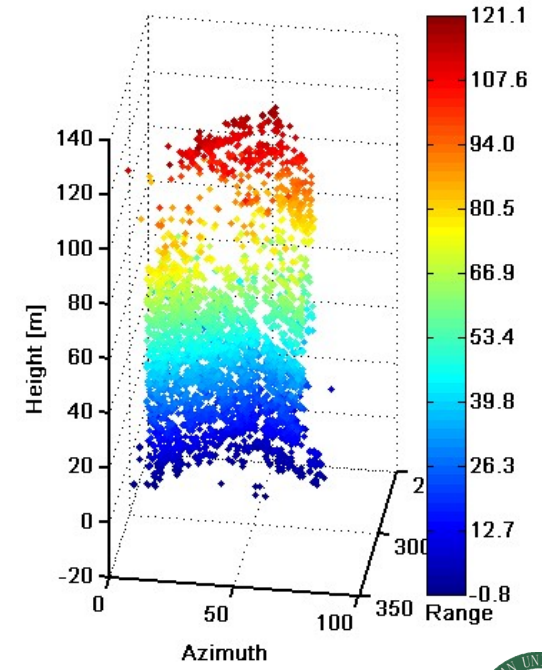
TSVD, Twist & BP



TSVD



TWIST

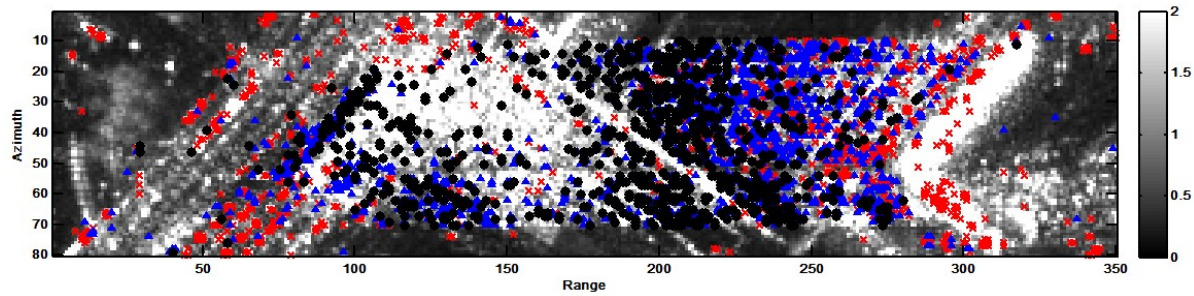


BP

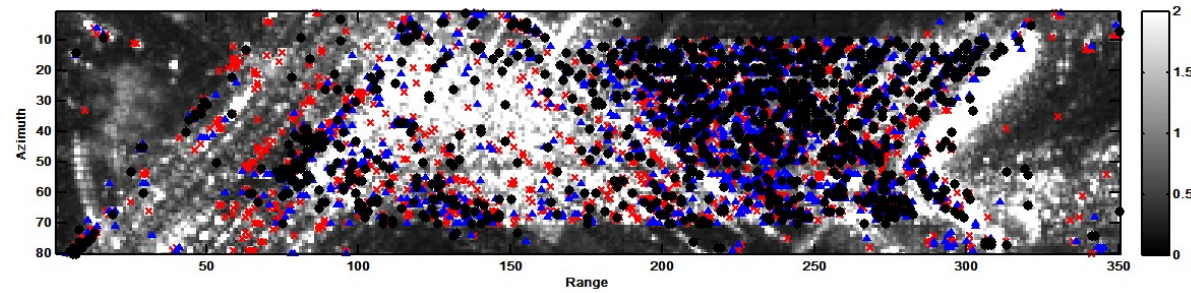


TSVD, Twist & BP

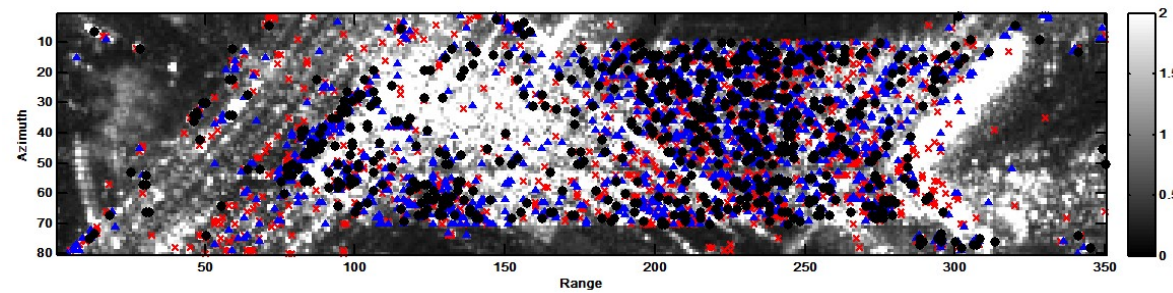
(a) TSVD
85 seconds



(b) TWIST
89 seconds



(c) BP
1378
seconds



red: single;
blue: double;
black: multi



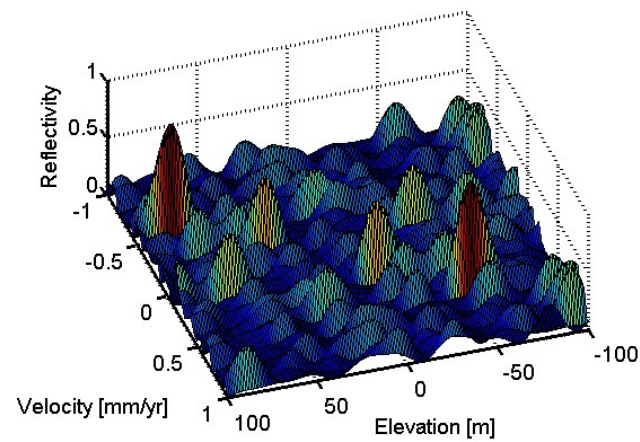
Differential TomoSAR

- Extend the model to the time-domain and include an estimation of the deformation
 - 4D TomoSAR
- Basically just an extension of the previously described method
 - Including an additional dimension for the focusing
- Can be further extended by including seasonal motion
 - Sometimes called 5D TomoSAR

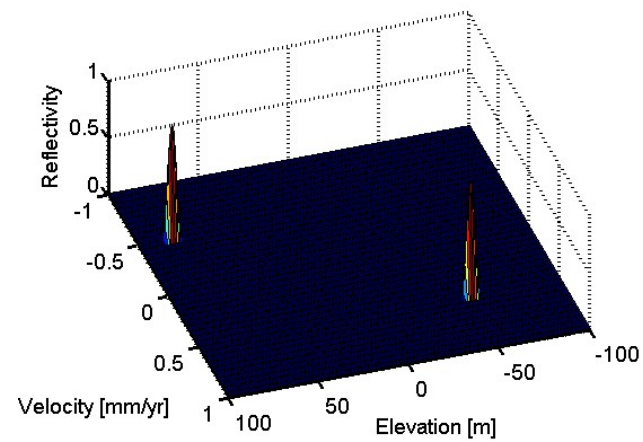


D-TomoSAR

Simulation results:



BSVD



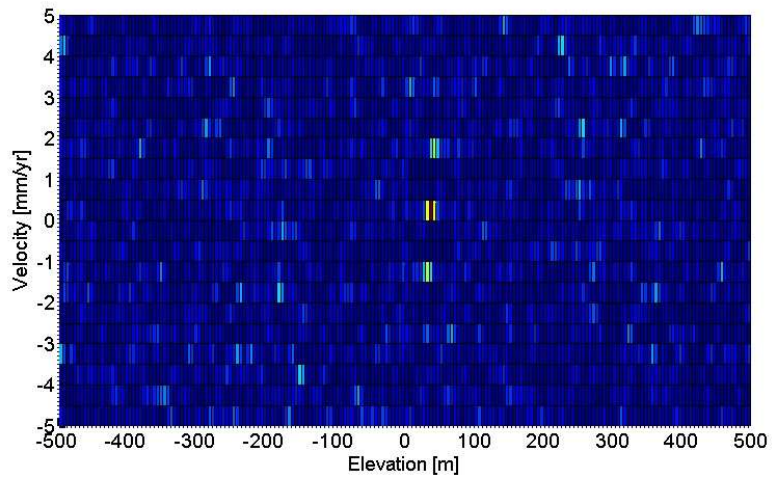
TWIST

= for D-TomoSAR, the noise suppression gets even more important

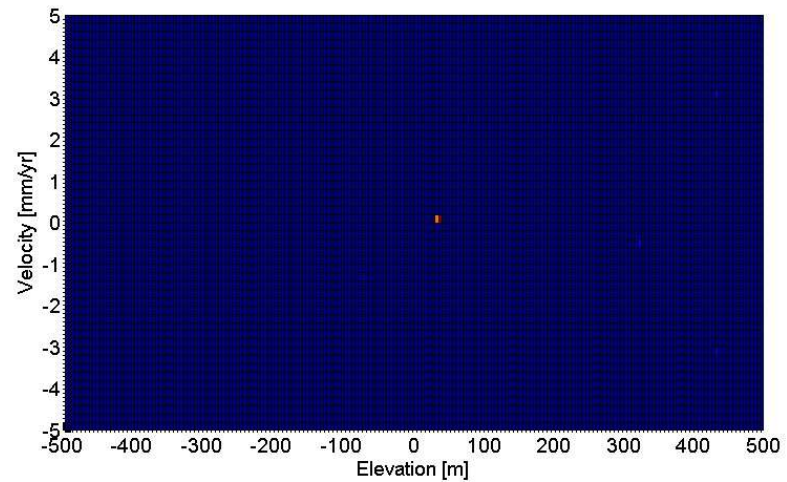


D-TomoSAR

Example: TSX stack from Las Vegas:



BSVD



TWIST

= clear result in TWIST



Practical implementations

Due to the high computational demand for compressive sensing TomoSAR, the processing can be divided:

1. PS-InSAR for pre-processing – APS estimation
2. Basic TomoSAR processing for model estimation
3. Depending on the number of scatterers:
 - One scatterer per resolution cell: use PS-InSAR for processing
 - Two or more scatterer: use TomoSAR

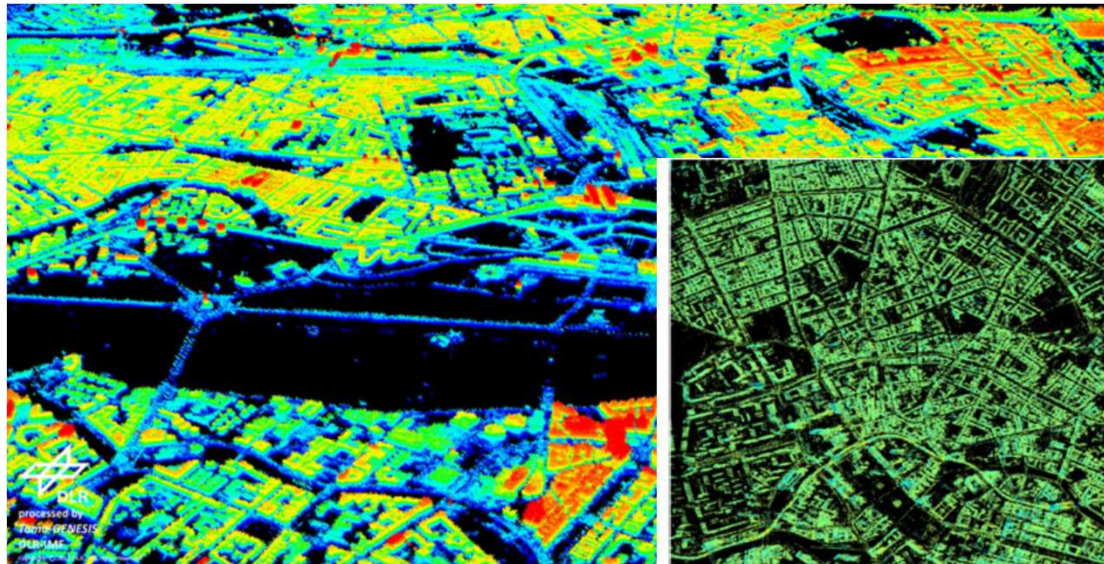


Geodetic SAR tomography

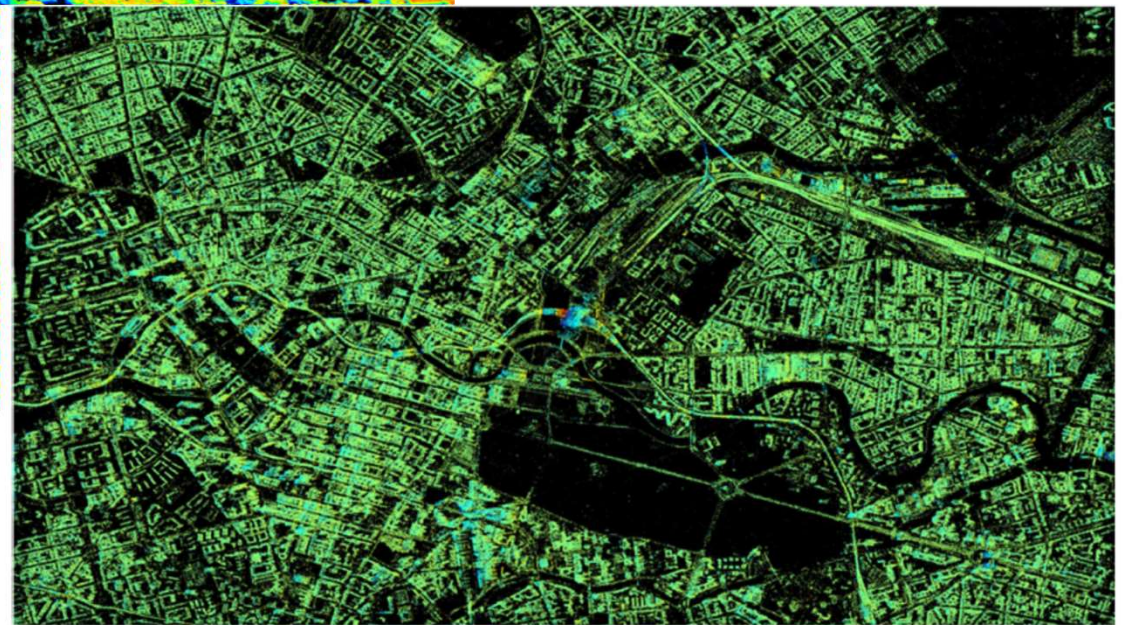
- Fusion of SAR imaging geodesy and TomoSAR
- SAR imaging geodesy:
 - Very high absolute geo-positioning capability of SAR
 - Especially with TerraSAR-X due to the very precise orbit
 - see Eineder et al, Cong et al, Balss et al....
- The fusion allows getting precise *absolute* 3D positions



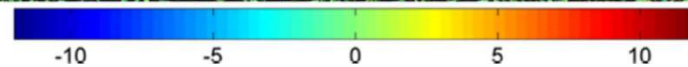
Geodetic SAR tomography



from Zhu et al, 2016 – 3D absolute positioned TomoSAR point cloud from Berlin



from Zhu et al, 2016 – Amplitude of the seasonal motion derived from one stack



References

- ❖ Reigber, A.; Moreira, A.; , "First demonstration of airborne SAR tomography using multibaseline L-band data," *Geoscience and Remote Sensing, IEEE Transactions on* , vol.38, no.5, pp.2142-2152, Sep 2000
- ❖ G. Fornaro, F. Serafino, and F. Soldovieri, "Three-dimensional focusing with multipass SAR data," *IEEE Trans. Geosci. Remote Sens.*, vol. 41, no. 3, pp. 507–517, Mar. 2003.
- ❖ F. Lombardini, "Differential tomography: a new framework for SAR interferometry," *IEEE Trans. Geosci. Remote Sens.*, vol. 43, no. 1, pp. 37–44, Jan. 2005.
- ❖ G. Fornaro and F. Serafino, "Imaging of Single and Double Scatterers in Urban Areas via SAR Tomography," *IEEE Trans. Geosci. Remote Sens.*, vol. 44, no. 12, pp. 3497–3505, Dec. 2006.
- ❖ F. Lombardini and M. Pardini, "3-D SAR Tomography: The Multibaseline Sector Interpolation Approach," *IEEE Geosci. Remote Sens. Lett.*, vol. 5, no. 4, pp. 630–634, Oct. 2008.
- ❖ G. Fornaro, D. Reale, and F. Serafino, "Four-Dimensional SAR Imaging for Height Estimation and Monitoring of Single and Double Scatterers," *IEEE Trans. Geosci. Remote Sens.*, vol. 47, no. 1, pp. 224–237, Jan. 2009.
- ❖ X. X. Zhu and R. Bamler, "Tomographic SAR Inversion by L1-Norm Regularization—The Compressive Sensing Approach," *IEEE Trans. Geosci. Remote Sens.*, vol. 48, no. 10, pp. 3839–3846, Oct. 2010.
- ❖ X. X. Zhu and R. Bamler, "Let's Do the Time Warp: Multicomponent Nonlinear Motion Estimation in Differential SAR Tomography," *IEEE Geosci. Remote Sens. Lett.*, vol. 8, no. 4, pp. 735–739, 2011.
- ❖ X. X. Zhu and R. Bamler, "Very High Resolution Spaceborne SAR Tomography in Urban Environment," *IEEE Trans. Geosci. Remote Sens.*, vol. 48, no. 12, pp. 4296–4308, 2010.
- ❖ X. X. Zhu and R. Bamler, "Super-Resolution Power and Robustness of Compressive Sensing for Spectral Estimation With Application to Spaceborne Tomographic SAR," *IEEE Trans. Geosci. Remote Sens.*, vol. 50, no. 1, pp. 247–258, 2011.
- ❖ X. X. Zhu and R. Bamler, "Demonstration of Super-Resolution for Tomographic SAR Imaging in Urban Environment," *IEEE Trans. Geosci. Remote Sens.*, vol. 50, no. 8, pp. 3150–3157, Aug. 2012.
- ❖ F. Lombardini and M. Pardini, "Superresolution Differential Tomography: Experiments on Identification of Multiple Scatterers in Spaceborne SAR Data," *IEEE Trans. Geosci. Remote Sens.*, vol. 50, no. 4, pp. 1117–1129, 2012.
- ❖ D. Reale, G. Fornaro, and A. Pauciuolo, "Extension of 4-D SAR Imaging to the Monitoring of Thermally Dilating Scatterers," *IEEE Trans. Geosci. Remote Sens.*, vol. 51, no. 12, pp. 5296–5306, 2013.
- ❖ G. Fornaro, A. Pauciuolo, D. Reale, and S. Verde, "Multilook SAR Tomography for 3-D Reconstruction and Monitoring of Single Structures Applied to COSMO-SKYMED Data," *IEEE J. Sel. Top. Appl. Earth Obs. Remote Sens.*, vol. 7, no. 7, pp. 2776–2785, Jul. 2014.
- ❖ X. X. Zhu, S. Montazeri, C. Gisinger, R. F. Hanssen, and R. Bamler, "Geodetic SAR Tomography," *IEEE Trans. Geosci. Remote Sens.*, vol. 54, no. 1, pp. 18–35, Jan. 2016.



Tomographic scene reconstruction

Assuming typical airborne or spaceborne MB geometries, SAR Tomography can be formulated according to one simple principle:

Each focused SLC SAR image is obtained as the Fourier Transform of the scene complex reflectivity along the cross-range coordinate

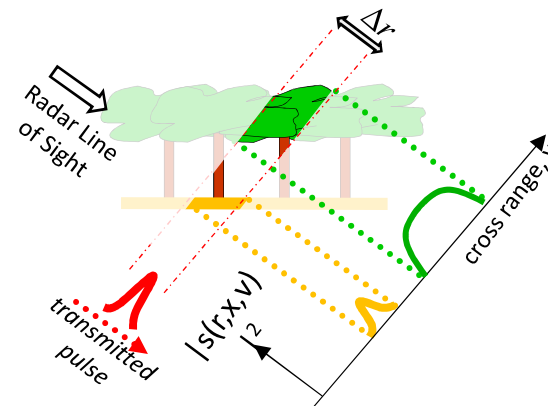
$$y_n(r, x) = \int s(r, x, v) \exp\left(-j \frac{4\pi}{\lambda r} b_n v\right) dv$$

$y_n(r, x)$: SLC pixel in the n -th image

$s(r, x, v)$: average complex reflectivity of the scene within the SAR 2D resolution cell at (r, x)

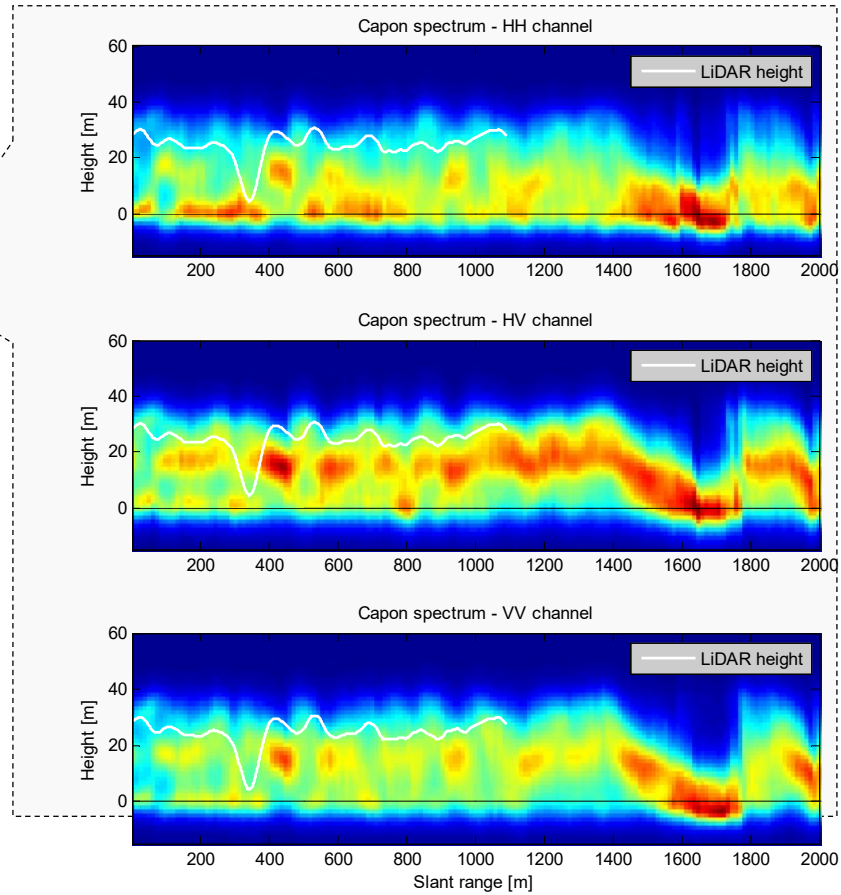
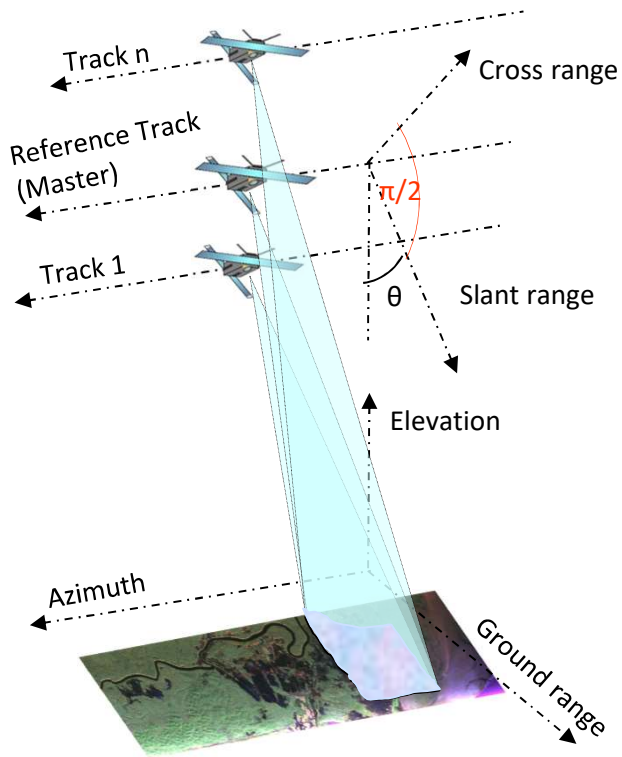
b_n : normal baseline for the n -th image

λ : carrier wavelength



⇒ The cross-range distribution of the complex reflectivity can be retrieved through Fourier-based techniques

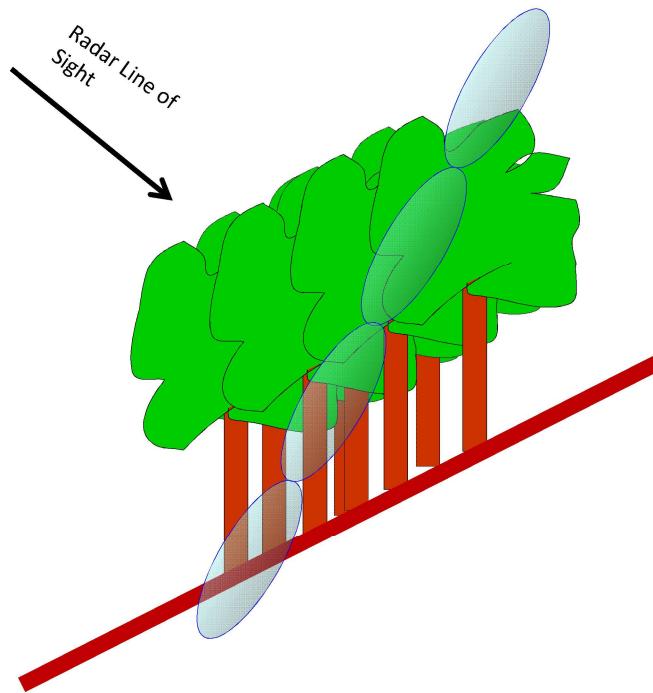
BIOMASS tomographic phase



Source:
Tebaldini & Rocca

Tomographic analysis: TropiSAR

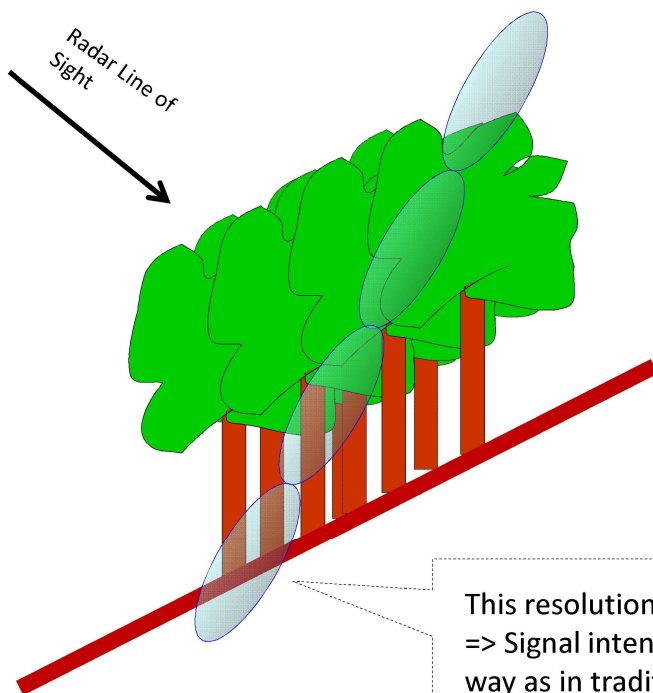
A closer look...



Source: Rocca

Tomographic analysis: TropiSAR

A closer look...

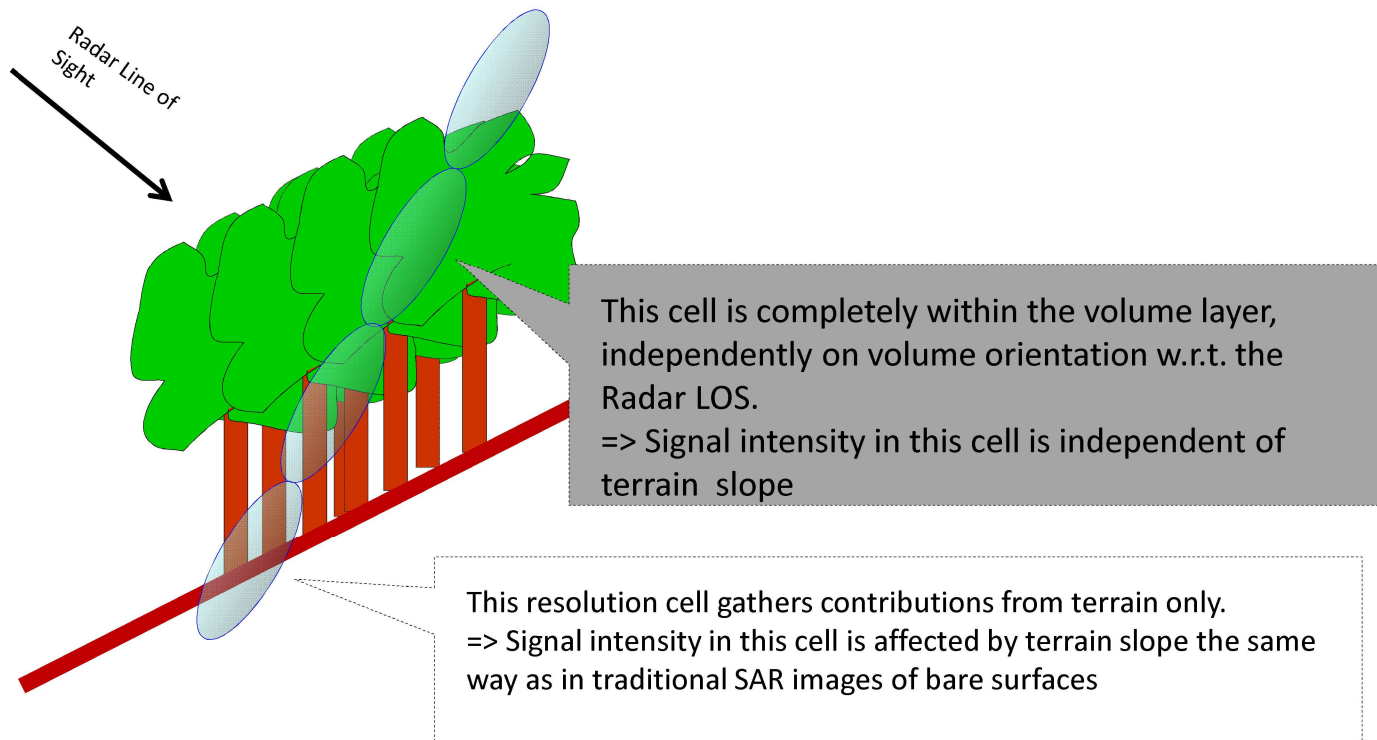


This resolution cell gathers contributions from terrain only.
=> Signal intensity in this cell is affected by terrain slope the same way as in traditional SAR images of bare surfaces

Source: Rocca

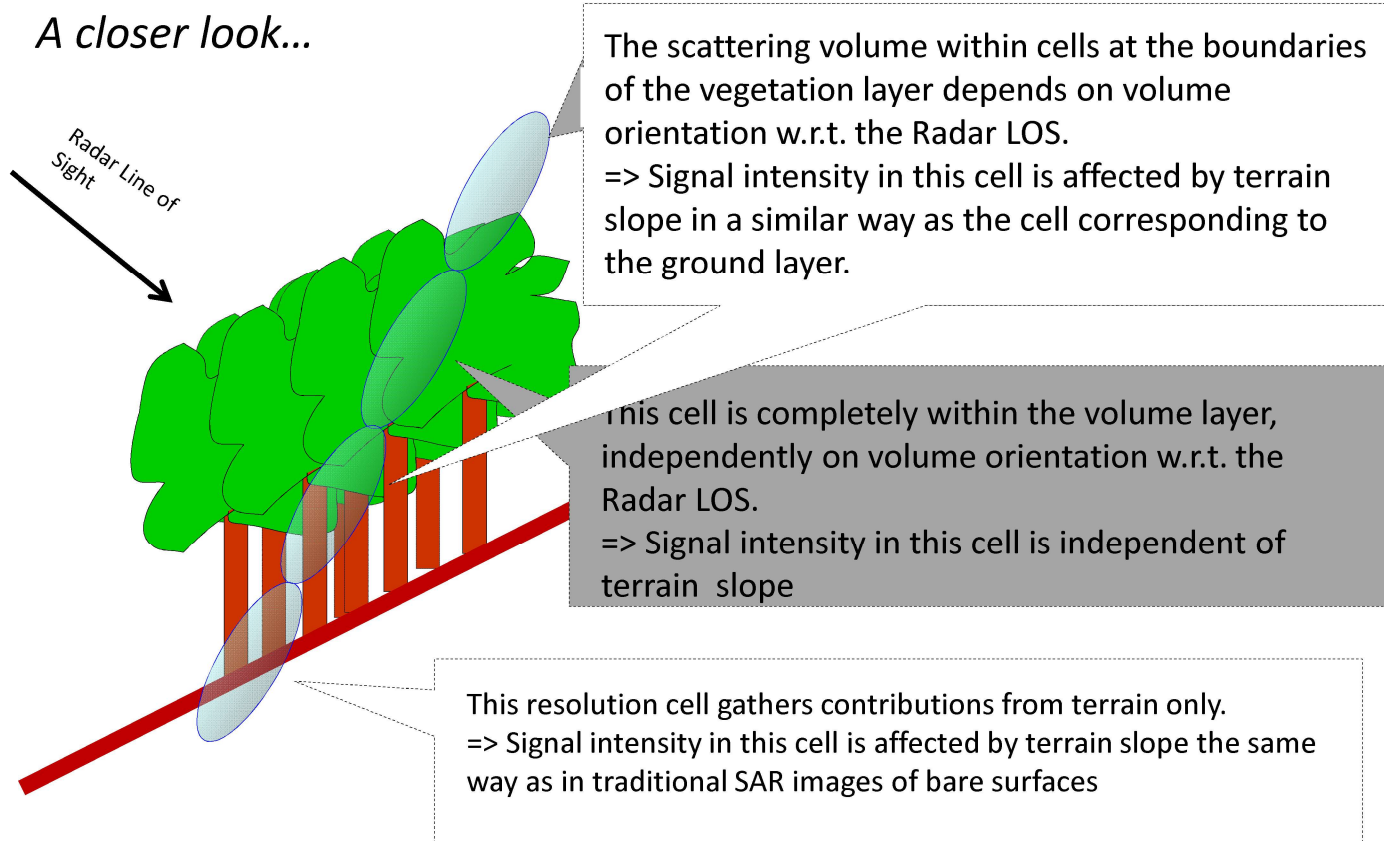
Tomographic analysis: TropiSAR

A closer look...



Source: Rocca

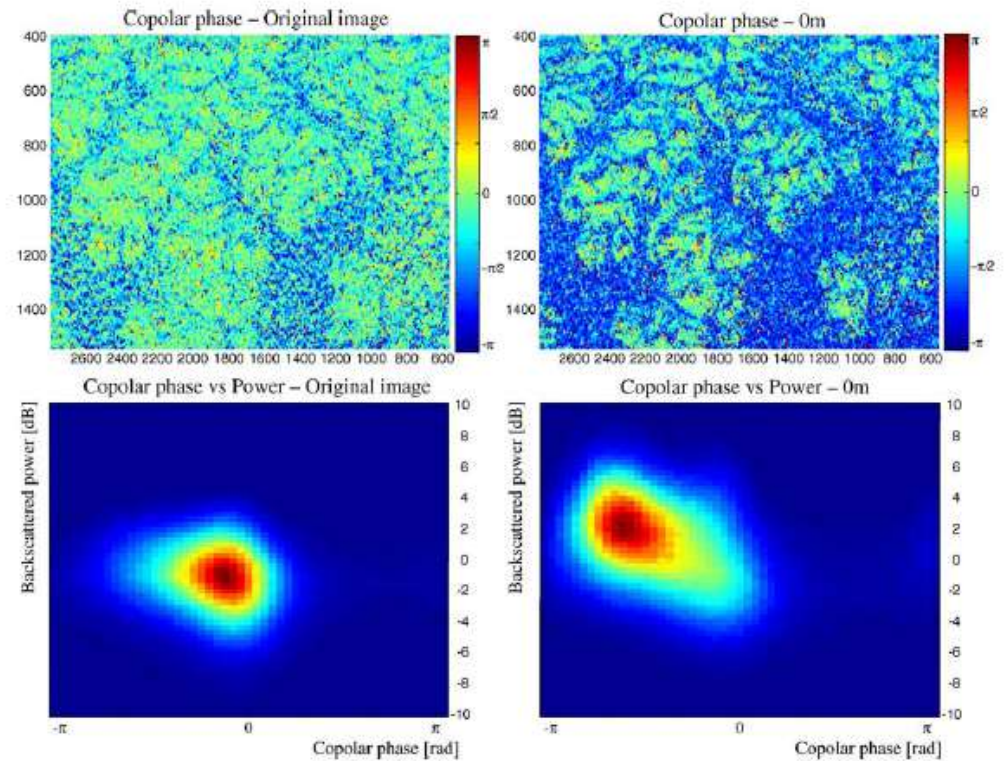
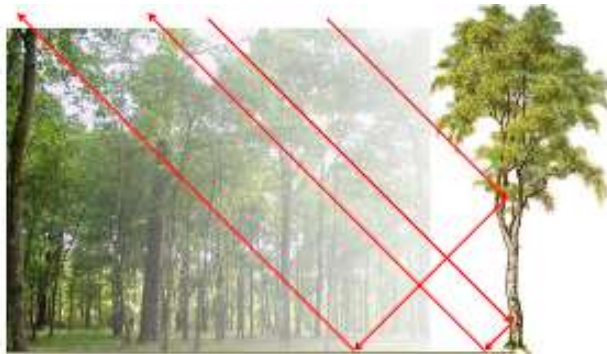
Tomographic analysis: TropiSAR



Source: Rocca

Tomographic analysis: TropiSAR

Co-polar signature at the ground layer reveals ground-trunk double bounce interactions dominate the signal from flat areas *despite* the presence of a 40 m dense tropical forest



Source: Rocca

Towards BIOMASS

- ❖ The scattering mechanisms at P-band in a very dense tropical forest:

Ground scattering is strongly visible and double bounces in flat terrain topography are visible everywhere.

Volume scattering is significantly related to the high range biomass

- ❖ It was found that scattering contributions from about 30 m above ground exhibit high sensitivity to forest biomass value ranging *from 250 t/ha to 450 t/ha*.

- ❖ SAR tomography allows to map not only **vertical forest structure** but also **biomass**.

Forest temporal decorrelation

P-band SAR tomography

key tool to *SEE* through the forest

suitable long wavelength to penetrate the dense forest

layer

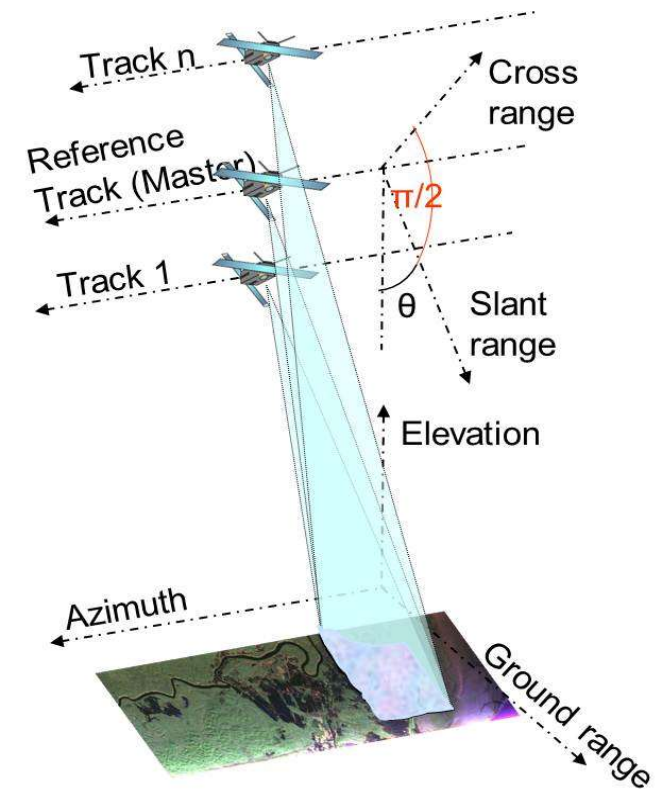
key indicator to tropical forest biomass

Orbit constraint: temporal decorrelation

Revisit time ≥ 1 day in a sun synchronous satellite configuration

Forest scattering changes with time

GOAL: Study the temporal decorrelation of scattering mechanisms of the radar signal in a tropical forest as a function of height and polarization.



References

Polarimetric and tomographic phenomenology of forests

- ❖ Reigber, A.; Moreira, A.; , "First demonstration of airborne SAR tomography using multibaseline L-band data," *Geoscience and Remote Sensing, IEEE Transactions on* , vol.38, no.5, pp.2142-2152, Sep 2000
- ❖ Mariotti d'Alessandro, M.; Tebaldini, S.; , "Phenomenology of P-Band Scattering From a Tropical Forest Through Three-Dimensional SAR Tomography," *Geoscience and Remote Sensing Letters, IEEE* , vol.9, no.3, pp.442-446, May 2012
- ❖ Frey, O.; Meier, E.; , "3-D Time-Domain SAR Imaging of a Forest Using Airborne Multibaseline Data at L- and P-Bands," *Geoscience and Remote Sensing, IEEE Transactions on* , vol.49, no.10, pp.3660-3664, Oct. 2011

Multi-layer optimization

- ❖ S. Sauer, L. Ferro-Famil, A. Reigber, E. Pottier, "Multi-aspect POL-InSAR 3D Urban Scene Reconstruction at L-Band", *Eusar 2008*
- ❖ Y. Huang, L. Ferro-Famil, A. Reigber, "Under Foliage Object Imaging Using SAR Tomography and Polarimetric Spectral Estimators", *Eusar 2010*

Coherence optimization

- ❖ M. Neumann, L. Ferro-Famil, A. Reigber, "Multibaseline Polarimetric SAR Interferometry Coherence Optimization", *IEEE Geoscience and Remote Sensing Letters*, 2008
- ❖ E. Colin, C. Titin-Schnaider, W. Tabbara, "An Interferometric Coherence Optimization Method in Radar Polarimetry for High-Resolution Imagery", *IEEE Transactions on Geoscience and Remote Sensing*, 2006

SKP decomposition: theory, algorithms and physical implications

- ❖ S. Tebaldini, "Algebraic Synthesis of Forest Scenarios from Multi-Baseline PolInSAR Data", *IEEE Transactions on Geoscience and Remote Sensing*, 2009
- ❖ Tebaldini, S.; Rocca, F.; , "Multibaseline Polarimetric SAR Tomography of a Boreal Forest at P- and L-Bands," *Geoscience and Remote Sensing, IEEE Transactions on* , vol.50, no.1, pp.232-246, Jan. 2012

Questions?

balz@whu.edu.cn

